RESEARCH ARTICLE

Island Arc WILEY

A major change in magma sources in late Mesozoic active margin of the circum-Sea of Japan domain: Geochemical constraints from late Paleozoic to Paleogene mafic dykes in the Sergeevka belt, southern Primorye, Russia

Victor P. Nechaev[1] | Evgene V. Sklyarov[2,3] | Yukio Isozaki[4] | Nikolay N. Kruk[5] | Alexey V. Travin[5] | Yukiyasu Tsutsumi[6] | Eugenia V. Nechaeva[3]

[1]Far East Geological Institute, Far Eastern Branch, Russian Academy of Sciences, Vladivostok, Russia

[2]Institute of the Earth's Crust, Siberian Branch, Russian Academy of Sciences, Irkutsk, Russia

[3]Polytechnic Institute, Far Eastern Federal University, Vladivostok, Russia

[4]Department of Earth Science and Astronomy, The University of Tokyo, Tokyo, Japan

[5]V. S. Sobolev Institute of Geology and Mineralogy, Siberian Branch, Russian Academy of Sciences, Novosibirsk, Russia

[6]Department of Geology and Paleontology, National Museum of Nature and Science, Tsukuba, Japan

Correspondence
Victor P. Nechaev, Far East Geological Institute, Far Eastern Branch, Russian Academy of Sciences, 159, Pr 100-let Vladivostoku, Vladivostok 690022, Russia.
Email: nechaev@fegi.ru

Funding information
Japan Society of Promoting Science, Ministry of Education, Grant/Award Number: 19H00711; Russian Foundation for Basic Research, Grant/Award Number: 19-05-00229; Russian Federation Government, Grant/Award Number: 075-15-2019-1883

Abstract

More than 30 mafic dykes crop out in the Sergeevka belt in the coastal South Primorye, Far East Russia, of which geologic settings have been unclear for years. This study conducted major- and trace elements characterization, Sr–Nd isotope analyses, and Ar–Ar amphibole and U–Pb zircon datings for these rocks in order to identify their origin. The results demonstrated that all dykes are characterized by high Ba/Yb and low Nb/Y, Zr/Y, and Th/Yb ratios, which suggest their origin from arc melts derived from thin wedge mantle and shallow-dipping slab. These dykes are clearly separated into two distinct age/geochemistry suites; that is, the Paleogene and Early Cretaceous one with dolerites/basalts and adakitic rocks, and the Permian–Triassic one with high-Mg and high-Al gabbro-dolerite varieties. Their geochemistry suggests that the older suite was sourced from a primitive depleted MORB mantle (DMM)-type mantle, whereas the younger suite from an enriched mantle II (EM2)-type mantle domain. The transition in source type from DMM to EM2 occurred during the Jurassic-earliest Cretaceous time, probably by a strong influence of a mantle plume onto the long-continuing subduction-related magmatism. The plume influence reached the maximum when the unique meimechite-picrite complex formed in the region.

KEYWORDS
gabbro-dolerite dykes, Greater South China, mantle plume, shallow subduction, South Primorye

1 | INTRODUCTION

Facing the Sea of Japan to the south, southern Primorye in Far East Russia geologically corresponds to the junction between the Central Asian orogenic belt (CAOB) and the Pacific-rim orogenic belt (*Nipponides*) (Ganbat et al., 2021; Isozaki, 2019; Khanchuk, 2001; Şengör & Natal'in, 1996; Xing et al., 2020; Figure 1). The geotectonic units in southern Primorye, in particular, the Sergeevka, Samarka, and Taukha belts on the east of the Khanka Massif represent the northern extensions of identical geotectonic units recognized in Japan (Golozoubov, 2006; Grebennikov et al., 2016; Ishiwatari & Tsujimori, 2003; Isozaki et al., 2014, 2017; Jahn et al., 2015; Khanchuk et al., 1996; Kojima et al., 2000), as they are composed of coeval subduction-related orogenic products, such as accretionary complex, blueschist, ophiolite, arc granitoid,
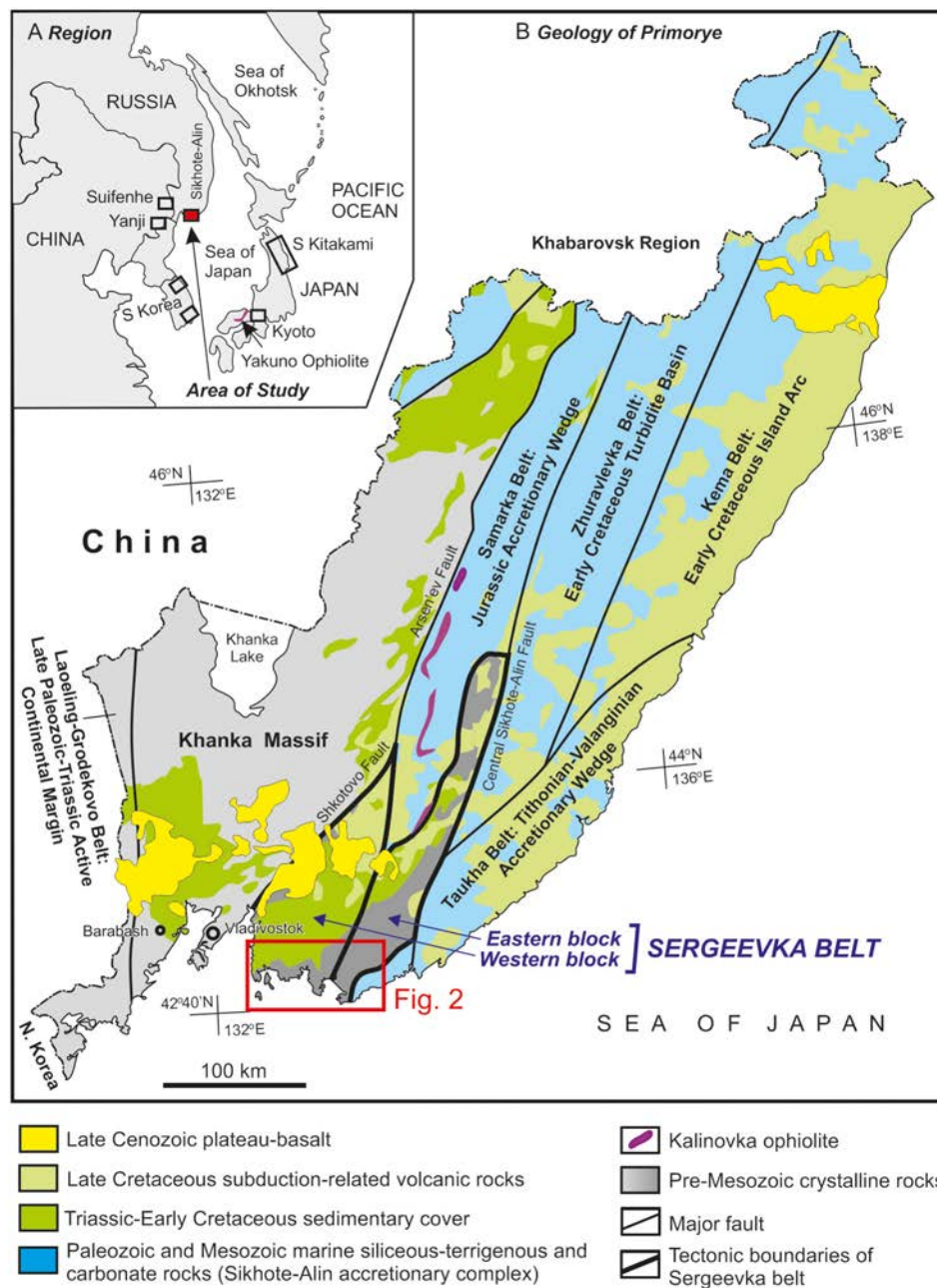
FIGURE 1 (a) Regional scheme with the location of the study area and other nearby districts of Paleozoic-Mesozoic and Paleocene-Eocene igneous activity; (b) geological sketch map of Primorye (modified after Nechaev et al., 2015) showing the study area

and shallow marine cover strata. In addition, these belts in southern Primorye were intruded by numerous Late Paleozoic to Paleogene dykes of diverse geochemistry (Chashchin et al., 2011; Gonevchuk et al., 1999; Govorov et al., 1997; Grebennikov et al., 2016; Kogan, 1976; Kruk, Golozoubov, Khanchuk, et al., 2018; Okamura et al., 1998, 2005; Prikhod'ko & Petukhova, 2011; Sayadyan et al., 1996; Shcheka, 1977; Wei et al., 2018; Wu et al., 2017). These dykes in Primorye are diverse not only in geochemistry; that is, from basalt to andesite/rhyolite, and with adakitic rocks, but also in age from Late Paleozoic to Paleogene, clearly older than the Miocene opening of the Sea of Japan. Therefore, they may likely have recorded the long-term secular change in magma nature along the same active continental margin.

The Sergeevka belt in southern Primorye represents a small remnant of the Paleozoic active continental margin along the eastern

margin of the Khanka Massif since the Paleozoic (Khanchuk et al., 1996). All of the Paleozoic and younger dyke rocks in this belt were formed likely under the long continuous subduction-relevant tectonic conditions. Since the neighboring belts on the ocean side are composed of the Jurassic and younger rocks (Figure 1), the relatively older dykes in the Sergeevka belt represent the early magmatic records in Primorye on the Pacific side of the Khanka Massif since the Paleozoic. Together with Mesozoic and Paleogene dykes in the same belt, we may reconstruct the secular change in magmatism for nearly 200 my within a single geotectonic domain.

To clarify the secular change in magma sources, we analyzed geochemical and geochronological characteristics of these dykes in the Sergeevka belt at 22 localities mostly along the southern coast. Our analyses determined their geochemistry, that is, compositions of

major, trace, and rare earth elements (REE), utilizing wet chemical and ICP-MS analyses, Sr–Nd isotopes analyses, and Ar–Ar amphibole and U–Pb zircon datings. By reporting the analytical results, this article discusses possible origin of dyke-generating magmas, and their secular change from the Permo–Triassic to Cretaceous–Paleogene time. We also compare the present results with those on similar dykes in other parts of southern Far East Russia, China, Korea, and Japan (e.g., Davis, 2003; Guo et al., 2007; Liu et al., 2012; Nechaev et al., 2018; Pouclet et al., 1995; Tsuchiya et al., 2005; Wu et al., 2017) for finding further geotectonic implications to the circum-Sea of Japan region. Previous studies assumed the subduction-related origin of these dykes and related volcanic and plutonic complexes; nonetheless, some emphasized possible links to large-scale strike-slip tectonics, including asthenospheric diapirism over 1000 km during the Cretaceous period (Grebennikov et al., 2016; Khanchuk et al., 2019; Martynov et al., 2016; Simanenko et al., 2002), and/or to a complicated plume influence onto the subduction system (Nechaev et al., 2018). We explore a more advanced tectono-magmatic model for the circum-Sea of Japan region during the late Paleozoic to Paleogene, particularly from the viewpoint of the newly proposed Greater South China continental block since the Paleozoic (Isozaki, 2019; Isozaki et al., 2017).

2 | GEOLOGICAL SETTING

The southern Primorye region of Far East Russia is basically composed of two major geologic entities, that is, the Khanka Massif and the Sikhote-Alin fold-and-thrust belt on the Pacific side (Figure 1; for example, Khanchuk et al., 1996). The former is composed of the Proterozoic and lower Paleozoic crystalline rocks; in contrast, the latter consists of Paleozoic-Mesozoic subduction-related orogenic units, that is, accretionary complexes, bluseschists, and ophiolites.

The Khanka Massif represents a southern part of the Bureya–Jiamusi–Khanka (BJK) crustal block or superterrane (Khanchuk, 2001; Khanchuk et al., 1996) with common signatures of the Pan-African (~600–500 Ma) metamorphism and magmatism (Zhou et al., 2010). The Proterozoic crystalline rocks were intruded by granitoids and adakites in multiple stages from the Ordovician to Paleogene (Kruk, Golozoubov, Kiselev, et al., 2018; Wu et al., 2017), which were covered by Paleozoic to Cenozoic volcano-sedimentary rocks that include Permian–Triassic arc volcanic rocks (Chashchin et al., 2020; Golozubov et al., 2017; Kruk et al., 2016), Lower Cretaceous and Cenozoic coal-bearing shallow- and non-marine strata, and Late Cenozoic intraplate basalts (Maksimov & Sakhno, 2008).

The Sikhote-Alin fold-and-thrust belt, on the east, is composed of several units of Mesozoic accretionary complexes (AC); for example, the Triassic-Jurassic ACs of the Samarka belt, Jurassic-Cretaceous ACs of the Taukha belt with fragments of pre-Jurassic oceanic lithosphere, and the Zhuravlevka, Kiselevka, and Kema ACs with fragments of pre-Cretaceous arc igneous complexes and back-arc basin sediments (Figure 1; Kemkin & Khanchuk, 1993; Kemkin et al., 1997, 1999; Nechaev et al., 1996, 1999; Kojima et al., 2000; Malinovsky

et al., 2008). All of the Sikhote-Alin ACs were intruded by mid-Cretaceous granitoids, and were also covered by Late Cretaceous calc-alkaline volcanic rocks and the Late Cenozoic tholeiitic and alkaline basalts (Golozoubov, 2006; Jahn et al., 2015; Khanchuk et al., 1996).

The Sergeevka belt occurs along the transitional domain between the Khanka Massif *sensu stricto* and the Sikhote-Alin fold-and-thrust belt (Figure 1). Its western margin is bounded by the northeast–southwest-trending Shkotovo Fault, whereas eastern margin is bounded by an unnamed low-angle fault, which puts the massif in contact with the structurally underlying Samarka belt (Golozoubov, 2006; Figure 2). This belt consists of the Early Paleozoic highly deformed metamorphic rocks (~460–490 Ma metamorphism and 460–520 Ma magmatism; Kruk, Golozoubov, Khanchuk, et al., 2018); for example, gneissose gabbro, diorite, and granitoids with xenoliths of Proterozoic schists plus amphibolites (~700–950, up to 2500 Ma; Kruk, Golozoubov, Khanchuk, et al., 2018), the middle-Paleozoic granitoids (~410–430 Ma; Kruk, Golozoubov, Khanchuk, et al., 2018), and the Permian–Triassic ophiolites associated with blueschists (~250 Ma for phengite and hornblende; Ishiwatari & Tsujimori, 2003). These igneous and metamorphic rocks are covered by Middle Paleozoic and Mesozoic volcano-sedimentary rocks of non- to shallow-marine facies (Figure 2; Golozoubov & Khanchuk, 2011; Nevolin et al., 2011). The Cambrian-Ordovician, Silurian-Devonian, and Permian–Triassic igneous rocks have typical subduction-related geochemical signatures, suggesting their origin in ancient active continental margins (Kruk, Golozoubov, Khanchuk, et al., 2018). On the other hand, the Albian-Cenomanian (mid-Cretaceous) basalts and andesites (Podolyan & Sedykh, 1997) have transitional geochemical signatures between subduction-related and intraplate types (Simanenko et al., 2002).

As shown in Figure 1, the Sergeevka belt along the southern Primorye coast occurs in two blocks; that is, eastern and western blocks. Traditional studies (e.g., Mel'nikov & Izosov, 1984) regarded the eastern block of the belt belongs to the Sikhote-Alin fold-and-thrust belt, whereas the western block to the Khanka Massif *sensu lato*. Nonetheless, recent studies by Khanchuk et al. (1996, 2016), Golozoubov (2006), Golozoubov and Khanchuk (2011), and Kruk, Golozoubov, Khanchuk, et al. (2018) re-interpreted that the Sergeevka belt as a whole forms a large-scale allochthonous nappe emplaced over the Sikhote-Alin fold-and-thrust belt. Golozoubov et al. (1999) further suggested that the Sergeevka belt (terrane) had once located at least 15° latitudinally to the south of the current position, on the basis of the unique pre-Albian (Early Cretaceous) flora from the coal basins of the belt, which is similar to that in northeast Japan but distinct from those in southern Khanka Massif and northeast China.

3 | RESULTS

3.1 | Dyke description

Previous studies identified numerous dykes intruded into the pre-Paleogene units of the Sergeevka belt including the Putyatin Island
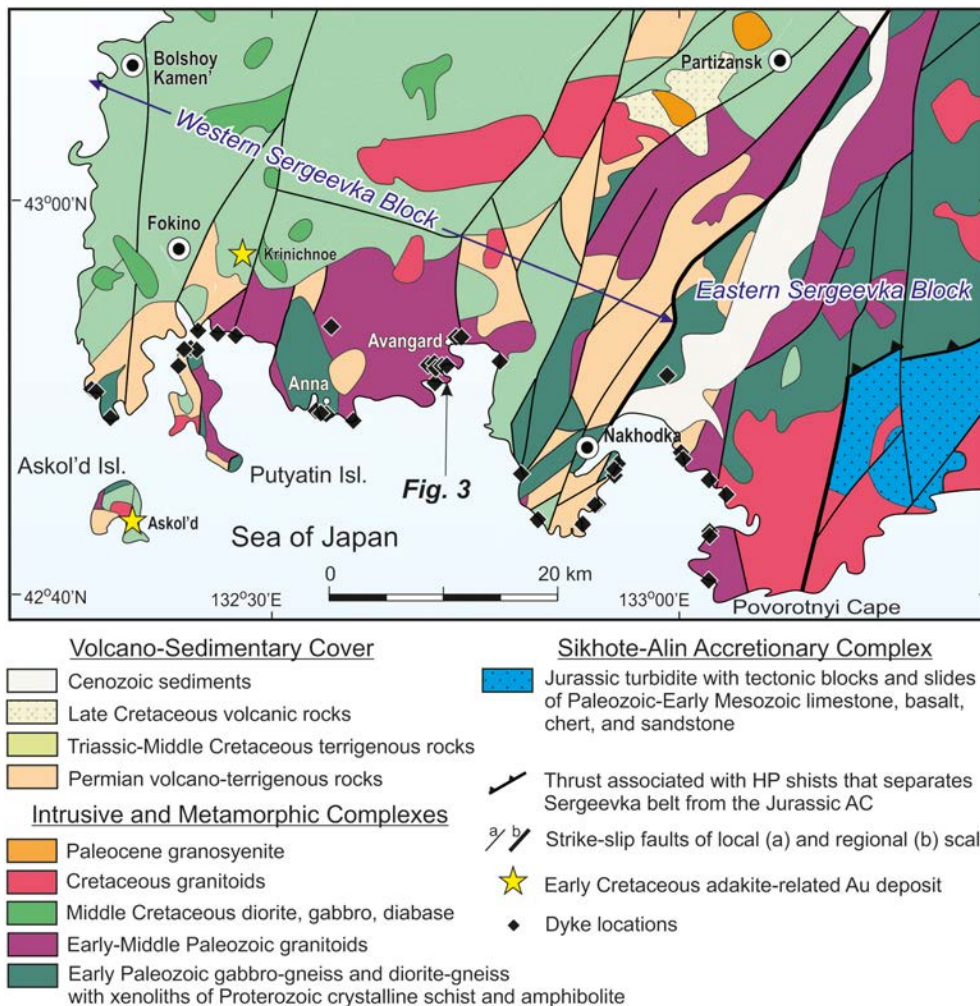
and the areas near Nakhodka (Kogan, 1976; Kruk, Golozoubov, Khanchuk, et al., 2018) and near the field camp of Far East Geological Institute at the Avangard Town on the southeastern part of the Tafuinsky granite massif (Nevolin et al., 2011; Figure 2). All the dykes are intruded into the early-middle Paleozoic granitoids, gabbros, and metasedimentary rocks and also the Permian volcanic rocks. These dykes are commonly of mafic composition, sometimes associated with single dykes of intermediate-felsic composition. Their thickness varies from 0.2 to 20 m, the shape changes from single, straight-lined to curving and branching, dipping angle—from subvertical to subhorizontal, strike—from northeast–southwest, conformable with rock bedding and/or cleavage to northwest–southeast, cross-cutting the visible tectonic structures and lithological boundaries.

The dykes of intermediate-felsic composition often show a unique lumpy structure that is related to their higher degree of alteration. The mafic rocks are represented by gabbro, dolerite and picrite. They commonly appear as single dykes with straight-lined contacts. However, the layered gabbro at the Avangard Site forms a branching dyke complex in the host Early Paleozoic granite. Contact zones of gabbro with granite consist of fine-grained dolerite that probably represents either a final phase of this intrusion or its quenching rim, or both. One of contacts of the dike complex is intruded by the dike of lumpy andesite.

In addition, Wei et al. (2018) recently studied several gabbroic dykes from the Avangard Site. Geochemical signatures such as tholeiitic composition, a right inclined REE pattern with the La/Yb ratio from 2.9 to 4.4, enrichment of large ion lithophile elements (LILE) and depletion of high field strength elements were considered to indicate the gabbro origin from partial melting of the primitive mantle material accreted to an active continental margin. The U–Pb dating of 5 zircon grains shows 123 ± 2 Ma interpreted as a magmatic age of the dyke, although other more abundant (23) zircon grains from the rock indicate a wide range of the ages from 240 to 2777 Ma (Wei et al., 2018).

3.2 | Analyzed rock samples

For various geochemical analyses, that is, major and trace element composition, Sr–Nd isotope ratios, Ar–Ar dating for amphiboles, and U–Pb dating for zircons, we collected 22 the least altered rock samples of dykes, all from the coastal outcrops in the study area between Bolshoy Kamen and Povorotnyi Cape, which locations are plotted in Figure 2. Refer to Supporting Information S2 for more details of these localities, such as longitude/latitude coordinates. They range in age

widely, from the Permian to Paleogene, suggesting multiple magmatic episodes in the Sergeevka belt during that time.

The analyzed 22 dykes have wide range in width and in composition from mafic to felsic, and mafic ones dominate over intermediate and felsic ones. Figures 3 and 4 illustrate some examples of their field occurrences. The mafic dykes commonly form single or a series of parallel bodies (Figure 4c,d, respectively), thickness of which varies from 0.3–0.5 to 10 m, whereas the contacts are straight-lined or slightly curved (Figure 4f). Less commonly, they compose more complex, branching and cutting each other bodies, with massive coarse-grained (Figure 4d,e) or layered inner parts and darker fine-grained contact zones (Figure 3a–d,f). All the studied mafic dykes intrude into either the Permian felsic volcanic rocks (Sample SE4167A; in Figure 4f) or the Early Paleozoic gabbros (Samples SE3677A, SE3679, SE3691A, and SE4175A) and granitoids (other samples; in Figure 3b–e).

As illustrated in Figure 4A, one felsic dyke (Sample SE4141A) of 7 m wide penetrated the Early Paleozoic granitoid with planar contact surfaces. The dyke of intermediate composition (Samples SE3658A and SE4164B) is situated between the weathered Early Paleozoic aplite and one of the branches of the layered-gabbro dyke at the Avangard Site (Figure 3E). Its contact with the hosting aplite includes a thin (1–3 cm) quenching zone, while contact with the adjacent gabbro (left in Figure 3E) is highly tectonized.

Most of the mafic rocks are melanocratic, fine-grained and/or porphyritic, containing small (up to 1–2 mm) phenocrysts of hornblende, clinopyroxene, and plagioclase (albite and oligoclase) (e.g., Samples 3677A and 4155B; Figure 5). Gabbroic varieties are less common, representing the inner parts of relatively thick (over 1 m thick) dykes (e.g., Samples SE3683/3-4; Figure 5). They also consist of hornblende, clinopyroxene, and plagioclase, forming allotriomorphic texture. The less altered rocks contain abundant magmatic (primary) clinopyroxene and hornblende that allows classifying most of them as lamprophyre, spessartite in particular. Hornblende is a dominant mafic mineral in layered gabbro from the Avangard Site (Samples SE3683/3-5 and 14RF41/2-5; Figures 3 and 5), so that this rock may also be identified as appinite (Murphy, 2013). However, no example of "multiple and repeated injection of bimodal magma," typical for the appinitic complexes worldwide (Murphy, 2019), exists in South Primorye. Accessory phases of the mafic rocks include Cr-spinel, particularly abundant in the layered gabbro of the Avangard Site, as well as ilmenite, magnetite, apatite, titanite, and zircon. The mafic rocks are commonly altered, with secondary amphibole (actinolite), biotite/phlogopite, chlorite, epidote, albite, calcite, and rutile associated with the leucoxene aggregates.

The felsic and intermediate rocks are porphyric, with phenocrysts of alkali feldspar and plagioclase (albite and oligoclase), quartz,
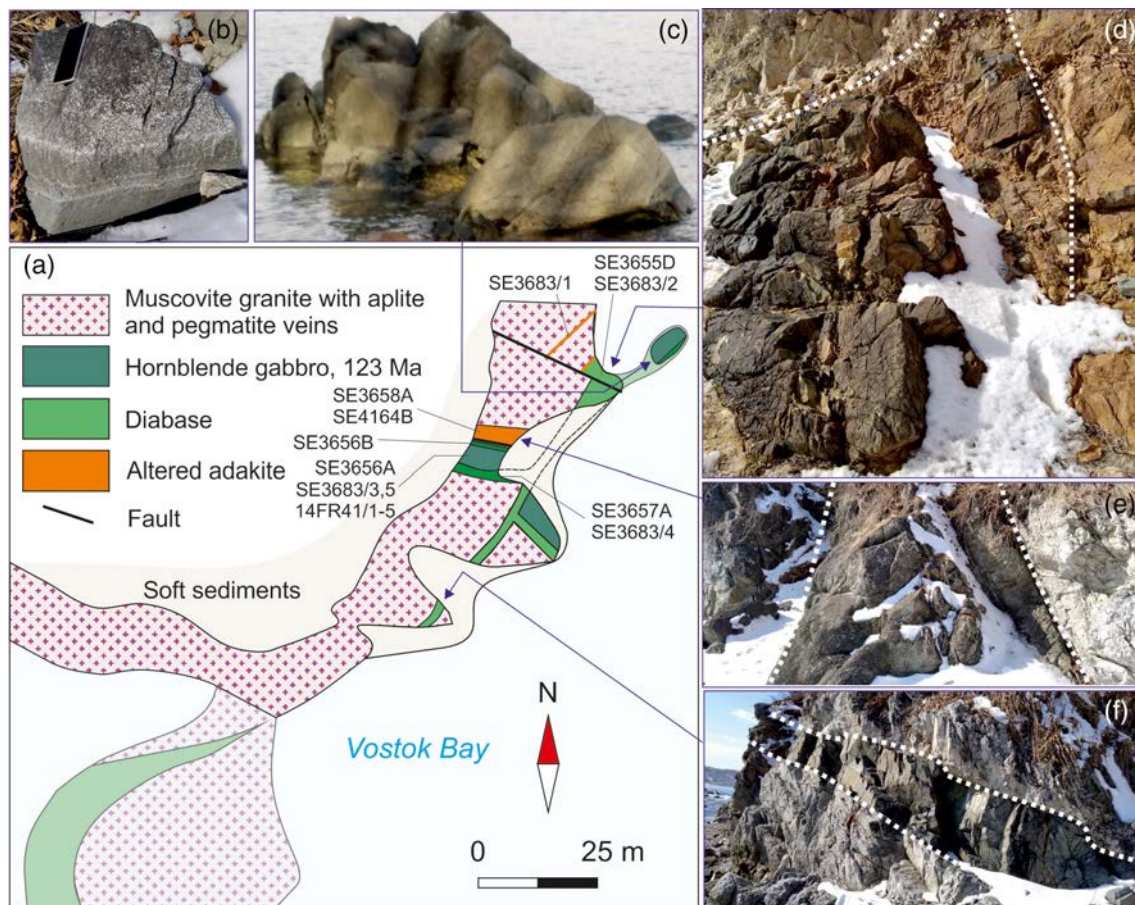

FIGURE 3 Geological sketch map for the Avangard Site showing the sample locations (a) and field photographs of a layered gabbro boulder (b) and dykes (c–f)
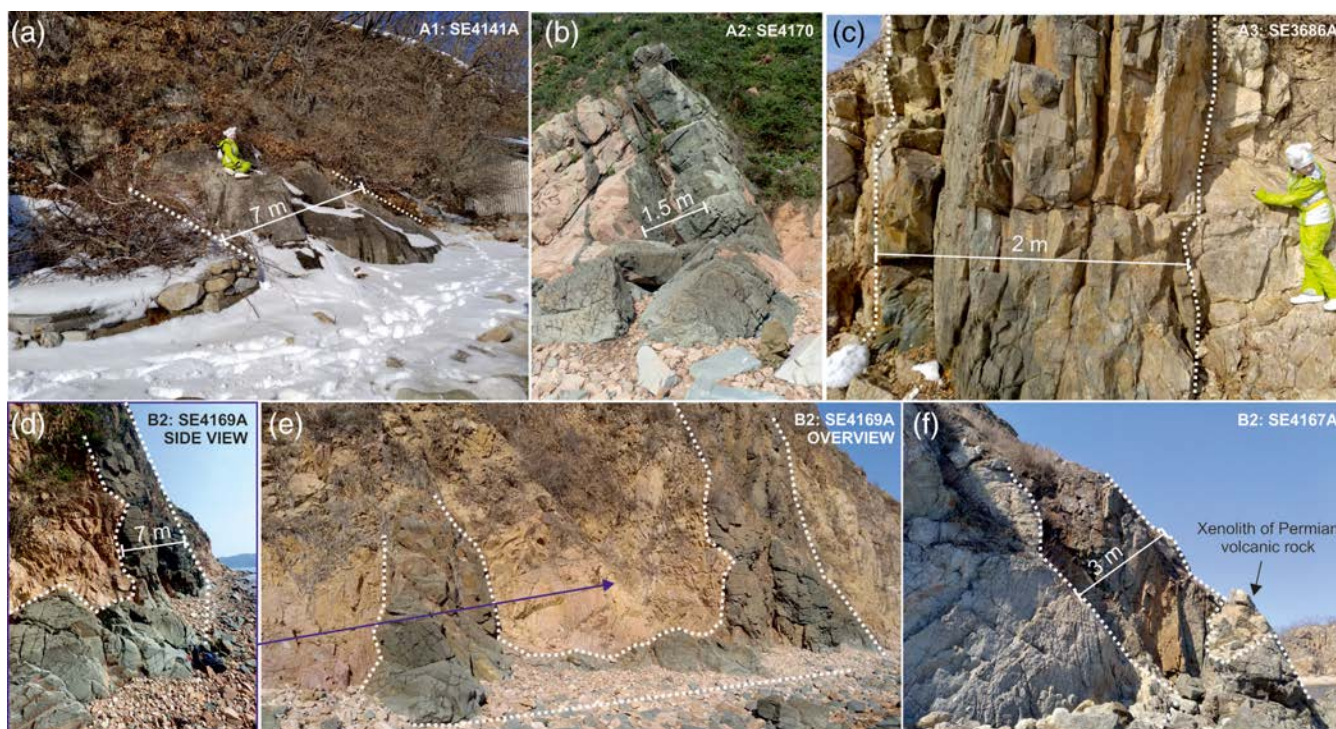
FIGURE 4 Field photographs of some dykes intruding the Early Paleozoic granites (a–e) and the Permian felsic volcanic rocks (f) in the study area. Labels in the upper right corners indicate the rock group and sample number (see Table S1 and Figure 2 for sample location)

hornblende, biotite, muscovite and a strongly altered groundmass with abundant leucoxene aggregates (e.g., Samples SE4141A and SE4164B; Figure 5). Dacite of Sample SE4141A contains Ti-magnetite as a primary opaque mineral, while altered andesite associated with the layered gabbro at the Avangard Site (Samples SE3658A and SE4164B; Figure 3) bears remnants of Cr-spinel plus sulfides, in particular chalcopyrite, cobaltite and alloclasite, which are also observed as hydrothermal minerals in the Early Cretaceous ore-bearing adakites of the local gold deposits.

Among the checked dyke rocks, only samples of the least altered rocks have been analyzed by using geochemical and mineralogical techniques, including wet chemical determination of major oxides, and ICP-MS for trace elements (twenty-two rock samples), Sr–Nd isotopic analyses (four bulk rock samples), Ar–Ar dating of amphibole (one analysis), and U–Pb La–ICP MS dating of zircon (19 grains from 1 rock sample). Refer to Supporting Information S1 for details of the procedures of geochemical analyses and Supporting Information S2 for analyses.

3.3 | New geochemical/geochronological constraints to dykes

3.3.1 | Mineral chemistry

Clinopyroxenes

Clinopyroxenes (Table S5) occur mainly as relics preserved in the glomerocrysts of mafic rocks. They are represented by augite in the phenocryst cores and diopside in the rims. All of them are enriched in Mg (Mg# [Mg/(Mg + Fe) atomic ratio] = 0.77–0.88) and contain up to 1.15 wt.% Cr_2O_3. Concentrations of aluminum and titanium significantly vary; for example, TiO_2 from 2.1 to 0.2–0.8 wt.%. A weak crystal zoning is manifested by increasing concentrations of iron and calcium toward the crystal rims.

Amphiboles

Amphiboles (Table S6) may be distinguished between primary magmatic, crystallized directly from the melt and post-magmatic, formed during cooling of the mafic melt and/or hydrothermal low-grade metamorphism. The former is represented by brown hornblende, specifically tschermacitic hornblende in the layered gabbro of Avangard Site (Figure 3; Table S6). It is characterized by high content of Al_2O_3 (11–12 wt.%), TiO_2 (1–2.5 wt.%), and $Na_2O + K_2O$ (2.4–3.2 wt.%). The contents of Ti, Al, and alkalis, as well as Mg# decrease toward the crystal rims. The post-magmatic amphibole suite, which partly or completely replace the magmatic hornblende, is dominated by actinolite with low contents of aluminum (1.5–2.5 wt.%), titanium and alkalis, which Mg# is, however, higher than that of associated primary hornblende.

Cr-spinels

Cr-spinels (Table S7, Figure 6) are found in gabbro-dolerites and andesite of Avangard Site. In all the rocks, they occur in different forms: as fine well-crystallized inclusions in magmatic and post-magmatic amphiboles and chlorite (Figure 6a,c) and as larger corroded
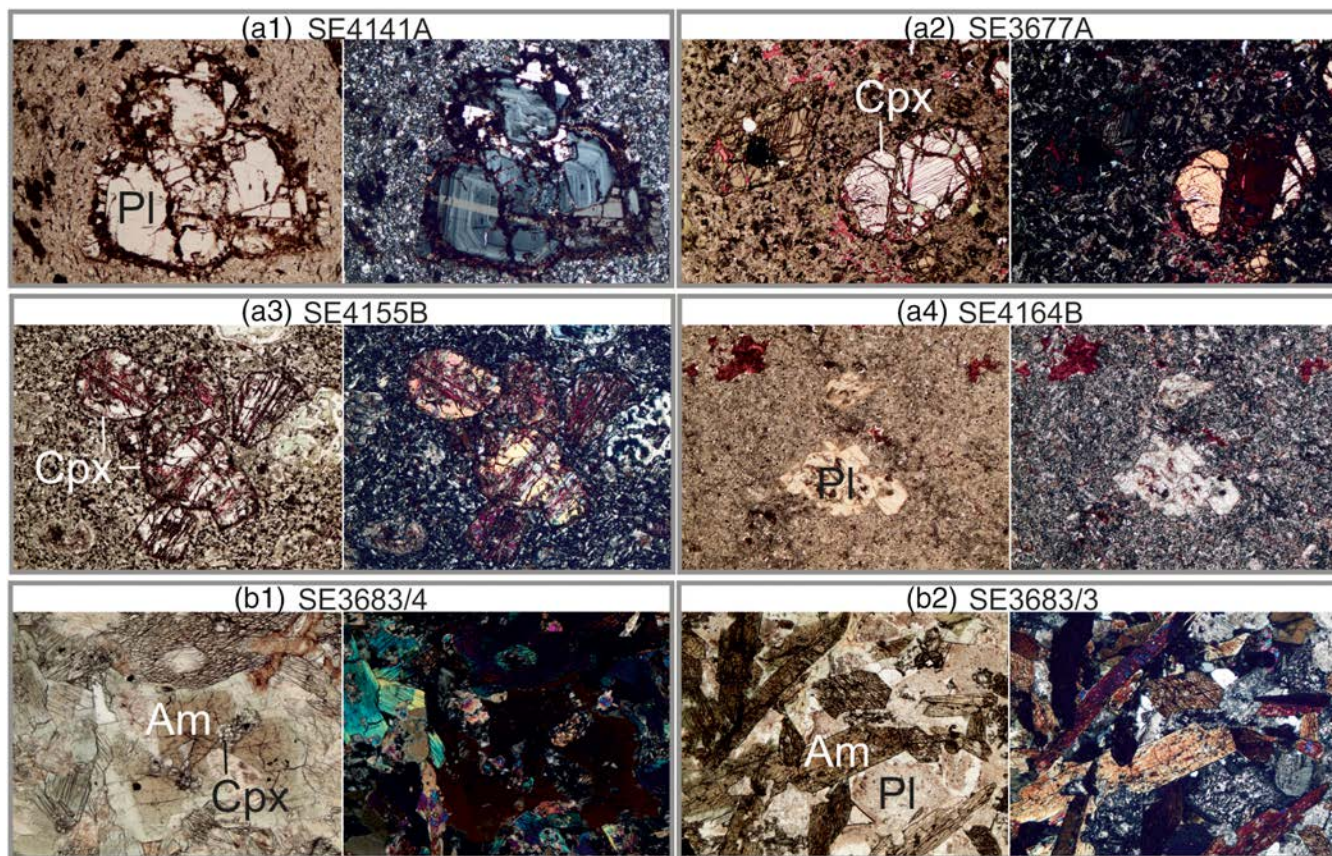
FIGURE 5 Microscopic images (3.18 × 2.27 mm, each) of the rock thin sections. Left, plane-polarized; right, cross-polarized: (group A1: Sample SE4141A) plagioclase porphyre; (A2: SE3677A) amphibole-clinopyroxene porphyrite; (A3: SE4155B) clinopyroxene porphyrite; (SE4164B, A4) highly altered plagioclase porphyrite with sericite pseudomorphs after plagioclase phenocrysts; (B1: SE3683/4) hornblende microgabbro; (B2: SE3683/3) hornblende gabbro. Pl, plagioclase; Am, amphibole; Cpx, clinopyroxene. The thin sections were dyed with alizarin, resulting in red color of calcite

(up to 180 µm) aggregates (Figure 6b). Chromite dissolution in amphibole was observed in some cases (Figure 6d). In the dolerites, Cr-spinel is widely variable in composition: Mg# = 0.1–0.48, Cr# [Cr/(Cr + Al) atomic ratio] = 0.38–0.56, Al# [Al/(Al + Fe^{3+}) atomic ratio] = 0.22–0.36, Fe^{3+}# [Fe^{3+}/(Fe^{3+}+Cr + Al) atomic ratio] = 0.08–0.34, with zoning best manifested by decreasing alumina and increasing magnetite components from core to rim. In the andesite, Cr-spinels with higher Cr# and Mg# (0.61–0.72 and 0.45–0.54, respectively) are characteristic, although rims of some grains have lower (0.08) Mg# (Table S7). Magnetite component is insignificant in the andesitic Cr-spinel.

Leucoxene
In well-crystallized forms (Table S8; Figure 7) is a characteristic feature of the studied andesite and dacite. Its content is highest in the most altered rock—andesite of the Avangard Site (Sample SE3658A). The leucoxene crystals of pseudocubic (Figure 7d,e), less commonly pyramidal shape is blue-gray and light-yellow in the hand specimen, while opaque or weakly translucent in red in thin sections under optical microscope. Their chemical composition varies widely (SiO_2 = 2–25 wt.%), although two varieties with 22 and 18 wt.% SiO_2 are most

common (Table S8). In addition to SiO_2 and TiO_2, the studied leucoxene contains FeO (2.5–4.4 wt.%), Al_2O_3 (0.8–1.7 wt.%) and CaO (0.25–0.39 wt.%), with a sporadic presence of MgO and K_2O. The "turtle back" texture caused by heterogeneous composition is common (Figure 7b). Zoned crystals are less common (Figure 7c). In Sample SE4141A, the TiO_2 phase is preserved in a core of the leucoxene crystal with rims formed by Ti-magnetite (Figure 7a). The adjacent crystal consists of leucoxene core and Ti-magnetite rims as well.

3.3.2 | Two distinct suites in geochemistry

The analyzed dyke rocks have wide compositional ranges from picrobasalt to dacite, most of which belong to calc-alkaline series typical for volcanic arcs (Figure 8; Table S1). The arc affinity (Zheng, 2019) of all the rocks is supported by LILE and light-REE (La/Yb = 10–64) enrichments, Nb-Ta and Ti troughs, and Pb and Sr peaks in the primitive mantle-normalized grid (Figure 9), and chondrite-normalized REE spider diagrams (Figure 10). However, end members of the compositional trends indicate high-Mg alkaline and adakitic-felsic melts that are peculiar for subduction-related magmas (Figure 8).
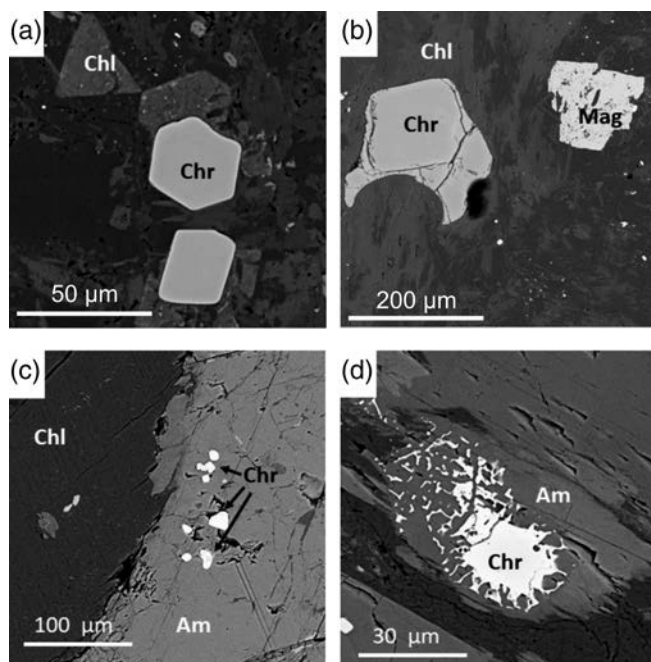
FIGURE 6 Back-scattered images of Cr-spinels. (a) and (b), andesite, samples SE3658B and SE3683-1, respectively; (c–d), dolerite, sample SE3684-4; all from the Avangard Site. Chr, Cr-spinel; Chl, chlorite; Am, amphibole; Mag, magnetite

Our new data (Table S1, Figure 8) allow the following two-fold subdivision of the dyke rocks of the Sergeevka belt; that is, Suite A and Suite B.

Suite A represents group of dyke rocks characterized by higher (7–9 or higher) La/Yb ratios; nonetheless they are heterogeneous. This includes the following 4 types; A1 to A4; namely, adakitic dacite such as Sample SE4141A with Sr/Y = 85.7, Y = 7.7; La/Yb = 60.5, Yb = 0.5; Figure 4 (A1 type); high-K calc-alkaline dolerite and basalt (A2 type); low-K calc-alkaline dolerite and picrite (A3 type); andesite dyke associated with the layered gabbro (A4 type) such as that at the Avangard Site (Samples SE3683/1, SE3658A and SE4164B; Figure 3).

In contrast, Suite B represents group of dykes with more homogenous chemistry characterized by lower (7–9 or lower) La/Yb ratio. This suite includes two types, that is, high-Mg appinitic gabbro-dolerite and picrite with MgO > 14 wt.% (B1 type), for example, Sample 3683/4 (Figure 5) at the Avangard Site (Figure 3), and high-Al dolerite and picrite with Al_2O_3 > 14 wt.% (B2 type). Most of them are calc-alkaline gabbro-dolerite. However, their low-SiO_2 (less than 45 wt.%) varieties have a relatively high K_2O content and may belong to alkaline series (Figure 8). In addition to the lower La/Yb ratio, these two groups of Suite B are distinguished from Suite A by the lower Th and U concentrations (Table S1; Figure 9) and much weaker light-REE enrichment (Figure 10).

In summary, geochemical differences among the distinguished types are as follows. The A1-type adakitic dacite is different from A2 and A3 types in silica content (Figure 8). The higher SiO_2 concentrations are also characteristic of adakitic andesites of A4 type. The felsic rocks in these groups often have high Sr/Y and La/Yb ratios (>20) and other characteristics of high-silica (SiO_2 > 56 wt.%) adakites (Figure 8;
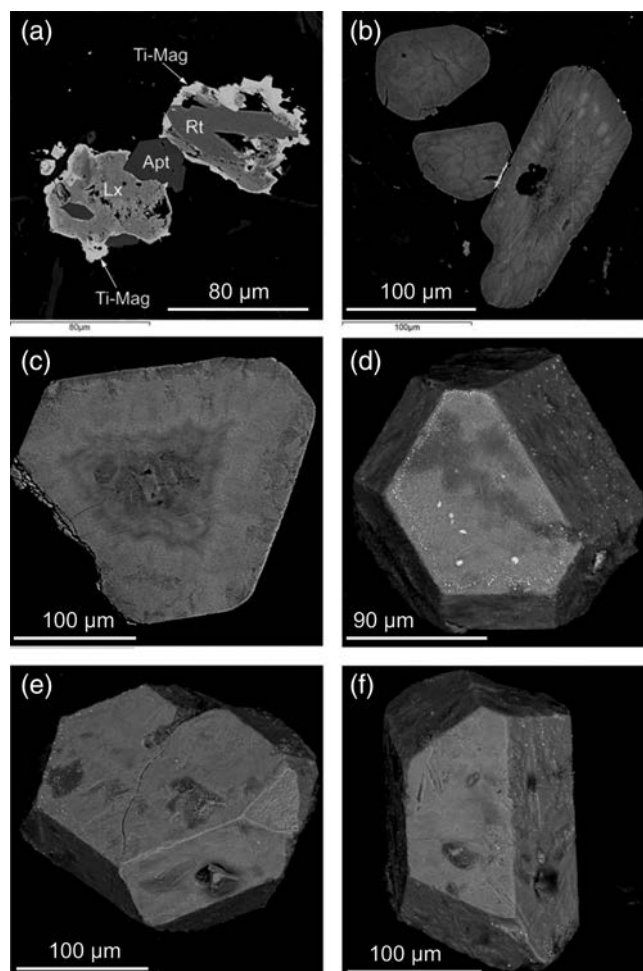

FIGURE 7 Back-scattered images of leucoxene and other Ti-phases in polished thin sections (a–c) and extracted grains (d–f). A, adakitic dacite, sample SE4141A, complex pseuodomorphs after Ti-phase composed of rutile (Rt), leucoxene (Lx) and Ti-magnetite (Ti-Mag); (b–f), andesite, sample SE3658A, the Avangard Site: (b) cluster of leucoxene grains with "turtle back" texture; (c) zoned leucoxene crystal; (d–f) leucoxene crystals

Moyen, 2009; Castillo, 2012; Wu et al., 2017). The A3 type is distinct from the A2 type in the absence of well-manifested Nb-Ta minimums at the primitive mantle-normalized diagrams (Figure 9; Table S1). The adakitic granitoids of Lower Cretaceous age (132–100 Ma) from small intrusions of the Krinichnoe and Askol'd gold deposits (Figure 2; Sayadyan et al., 1996; Gonevchuk et al., 1999; Wu et al., 2017) also belong to Group A4. They differ from the A1 adakite by a significantly smaller Nb-Ta minimum in the primitive mantle-normalized values (Figure 9). The B1 type is distinguished from B2 type and from all other studied rocks by anomalously high content of MgO. The B2 type has higher (relative to B1) Al_2O_3 values (Figure 8). A close relation of these two assemblages is clearly observed at the Avangard Site (Figures 3 and 4), where the low-Mg gabbro represented by Sample SE-3683/3 forms one of the dyke layers, while other samples from the same dyke have high-Mg compositions (Samples SE3683-2,4 and 14RF-2-5, Table S1).

FIGURE 8 Hacker classification and Sr/Y-La/Yb diagrams showing plots of the studied rocks and associated gabbro, basalt and adakite, all from the study area. Data for the associated rocks are from Gonevchuk et al. (1999), Okamura et al. (2005), Wu et al. (2017), and Wei et al. (2018). Fields for adakite and normal arc andesite-dacite-rhyolite assemblage are from Moyen (2009) and Ewart (1982), fields in the K_2O versus SiO_2 diagram and TAS (total alkali-silica) classification diagram are from Le Le Maitre (2002)
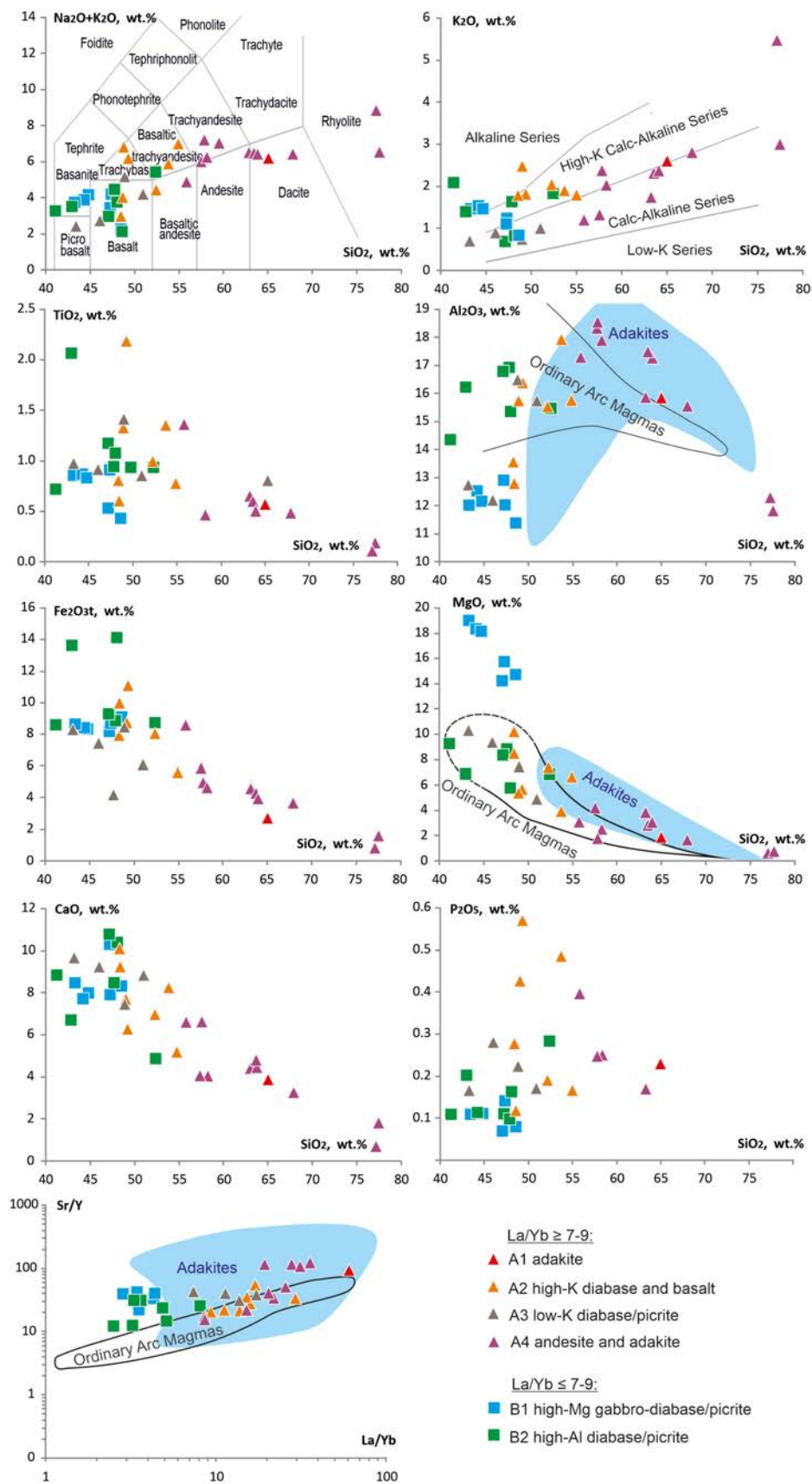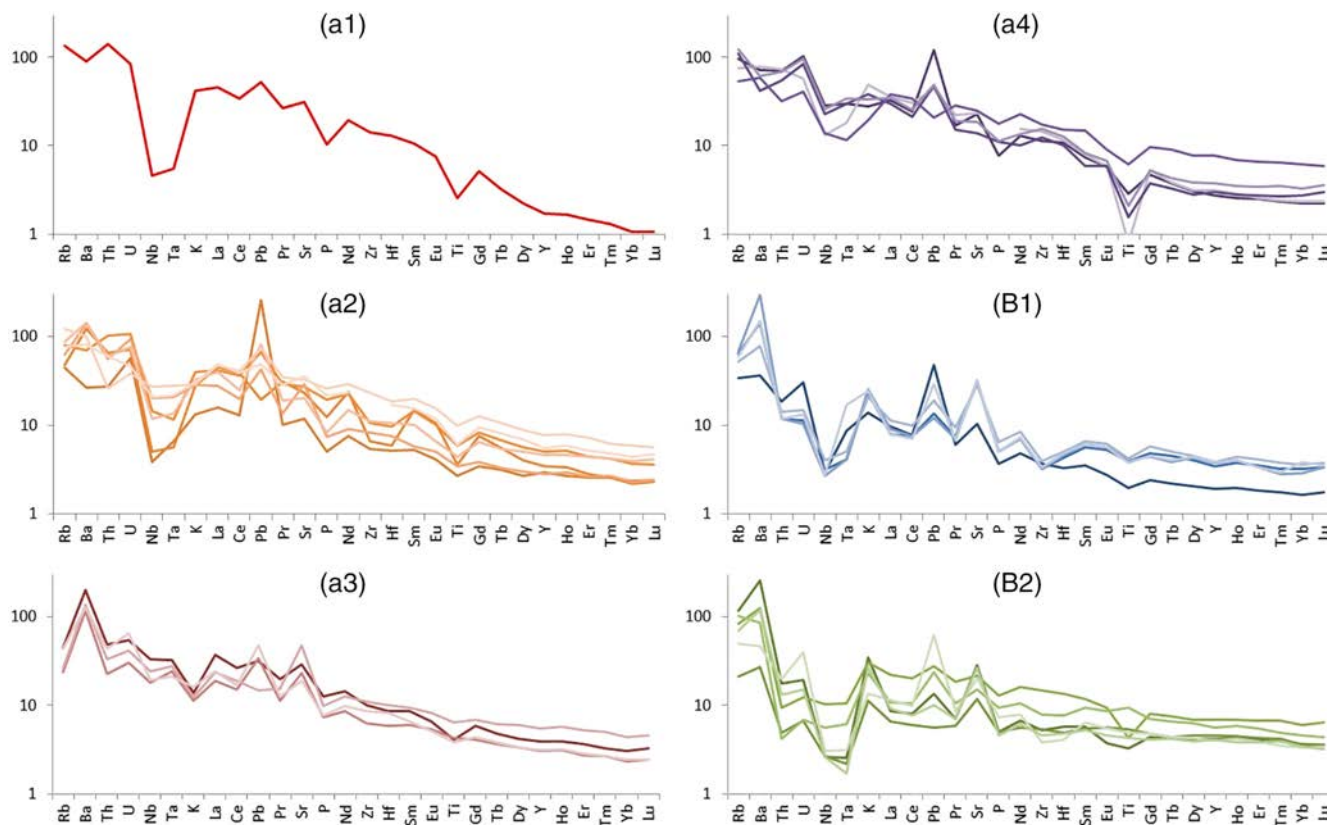
FIGURE 9 Primitive-mantle normalized multielemental plots for the investigated rocks with addition from Okamura et al. (2005), Wei et al. (2018), and Wu et al. (2017) on the primitive-mantle-normalized spider diagrams (after McDonough & Sun, 1995)

3.3.3 | Sr-Nd isotopic compositions

The obtained isotopic data (Table S2; Figure 11) fit well with compositional variations of the Paleogene and Early Cretaceous adakitic rock suites of the Sea-of-Japan region (Guo et al., 2009; Imaoka et al., 2017; Ji et al., 2007; Osozawa et al., 2019; Pouclet et al., 1995; Tsuchiya et al., 2005, 2007; Wu et al., 2017). They suggest that magma sources of the analyzed dykes and associated rocks may have included both depleted and enriched mantle domains, depleted MORB mantle (DMM) and enriched mantle II (EM2), respectively.

It must be mentioned, however, that our dataset includes evolved and altered rocks, which are not necessarily suitable for direct assessing of mantle source compositions. The high ISr (0.7052 and 0.7067) of the two A4 samples probably reflect interaction with crustal rocks and/or the effects of secondary hydrothermal processes. The relatively low ISr (initial $^{87}Sr/^{86}Sr$ ratio) and high $\varepsilon Nd(T)$ of the A1 dacite (0.7036 and 5.29, respectively) support that this is a "classical" adakite, that is, a product of slab melting processes.

The two samples of the B Suite (Table S2) are more suitable for assessing mantle source compositions, although their raised $^{87}Sr/^{86}Sr$ isotopic ratio (0.7063 and 0.7067) might also be due to the alteration that was defined by our petrographic study (see above).

The analyzed dyke rocks appear fresh; nonetheless they indeed have suffered secondary alterations in certain degree; alteration degree generally increases according to the rock composition toward intermediate

and felsic rock varieties (Figure 5). In this regard, the following discussion focuses solely on mafic and ultramafic rocks, and on Cr-spinels that may better preserve primary information of their initial melts. Our interpretations are based mostly on trace element ratios that are regarded the least mobile in post-magmatic hydrothermal alterations (Condie, 2005; Pearce, 1983; Pearce et al., 2005; Pearce & Reagan, 2019).

3.3.4 | Dating

The newly measured zircon U–Pb ages clarified three zircon populations, that is, 43–48 Ma, 47–51 Ma, and 49–52 Ma, in the A1 adakitic dyke (Figure 12). Nonetheless, these close age groups are difficult to separate from each other, thus we take an integral estimation of 48.4 ± 0.7 Ma that most probably reflect a magmatic age of the rock. It is noteworthy that this age may correspond to the previously reported zircon U–Pb ages from (58–55 Ma) of the adakitic suite in northeast China near the Japan Sea (Guo et al., 2007, 2009) to 46–40 Ma ages in Primorye and in South Korea (Chashchin et al., 2011; Kim et al., 2005; Wu et al., 2017), and also to 44–38 Ma ages in northeast Japan (Tsuchiya et al., 2005). A few of much older zircon grains (804.3 ± 7.3 and 530.5 ± 13.3 Ma; Table S3) are most likely from xenocrysts.

The obtained Ar–Ar dating of amphiboles from the layered B1 gabbro is unequivocal, showing the weighted plateau age 272.2
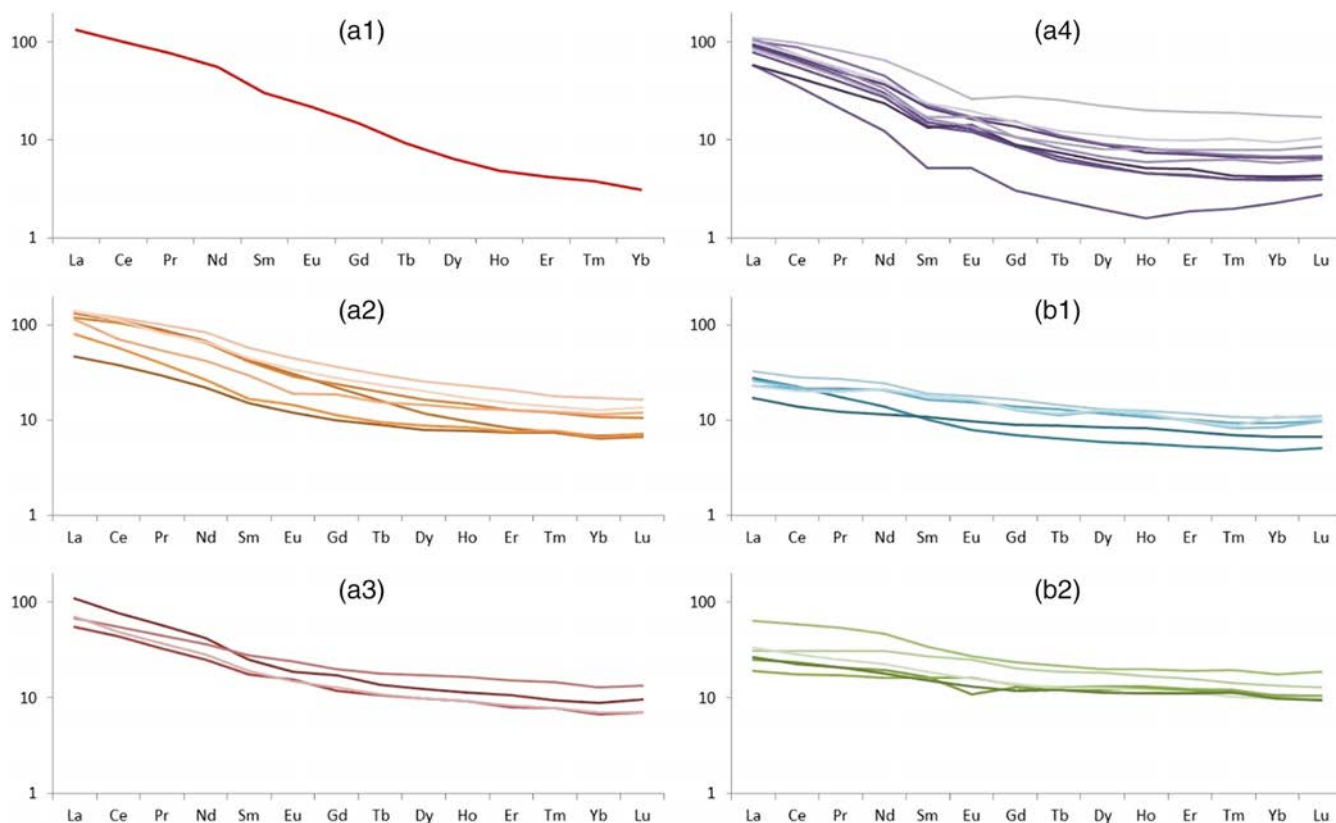
FIGURE 10 Chondrite-normalized REE spider diagrams (Sun & McDonough, 1989) showing geochemical differences between the groups of studied rocks with addition from Okamura et al. (2005), Wei et al. (2018), and Wu et al. (2017)
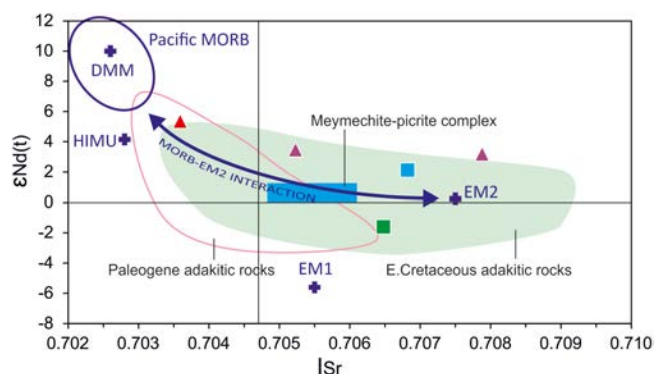

FIGURE 11 Sr-Nd isotopic compositions of the studied rocks with addition from Wu et al. (2017). Fields of the Paleogene and early Cretaceous adakitic rocks are also reported (Guo et al., 2009; Imaoka et al., 2017; Ji et al., 2007; Osozawa et al., 2019; Pouclet et al., 1995; Tsuchiya et al., 2005; Wu et al., 2017). The DMM, HIMU, EM1, EM2, and Pacific MORB compositions are from Hart (1988). See Figure 7 for symbols

± 9.5 Ma and the integral (total gas) age 223.7 ± 9.5 (Figure 13; Table S4). The former may indicate the Early-Middle Permian age of the main magmatic-amphibole crystallization phase that either continued as multi-phase magmatic crystallization or was partly altered in Late Triassic or later. Perhaps both processes took place since the dated gabbro from Group B1 have a layered structure

evidencing multi-phase magmatic activity and bear a secondary amphibole.

As mentioned above, Wei et al. (2018) presented results of U–Pb dating of zircon extracted for the B1-2 gabbro from the Avangard Site. Twenty-eight zircon grains have been analyzed in total, among which 5 zircon grains indicate 123 ± 2 Ma interpreted as a magmatic age of the dyke, while others indicate a wide range of the ages from 240 to 2777 Ma (Wei et al., 2018). Our attempt to extract zircon from the same gabbro has failed. The dates by Wei et al. (2018) do not correspond to the Ar–Ar dating of this study. In addition, such a wide age range of zircon is not common for a magmatic mantle-derived host. Judging from these, we regard the emphasized age of 123 Ma for this dyke by Wei et al. (2018) invalid, although this date corresponds to the probable age of the A4 rock group (note that the A4 andesite is closely associated with the B1 gabbro-dolerite at the Avangard Site, Figure 3).

In summary, the obtained ages characterize single dykes of the complex suites and, even with additions from Okamura et al. (2005), Wei et al. (2018) and Wu et al. (2017), are too few to reliably date all the A and B groups of studied rocks. As presented in the text above and in Table S1, these dates are: 48.4 Ma, U–Pb zircon age of adakitic dacite (A1, this study) and 54.8 Ma, K–Ar age of basalt (A2, Okamura et al., 2005); 100–132 Ma, K–Ar, Rb–Sr and U–Pb ages of gabbro-granitic complex from Krinichnoe and Askol'd gold-ore deposits (A4, Gonevchuk et al., 1999; Sayadyan et al., 1996; Wu et al., 2017);
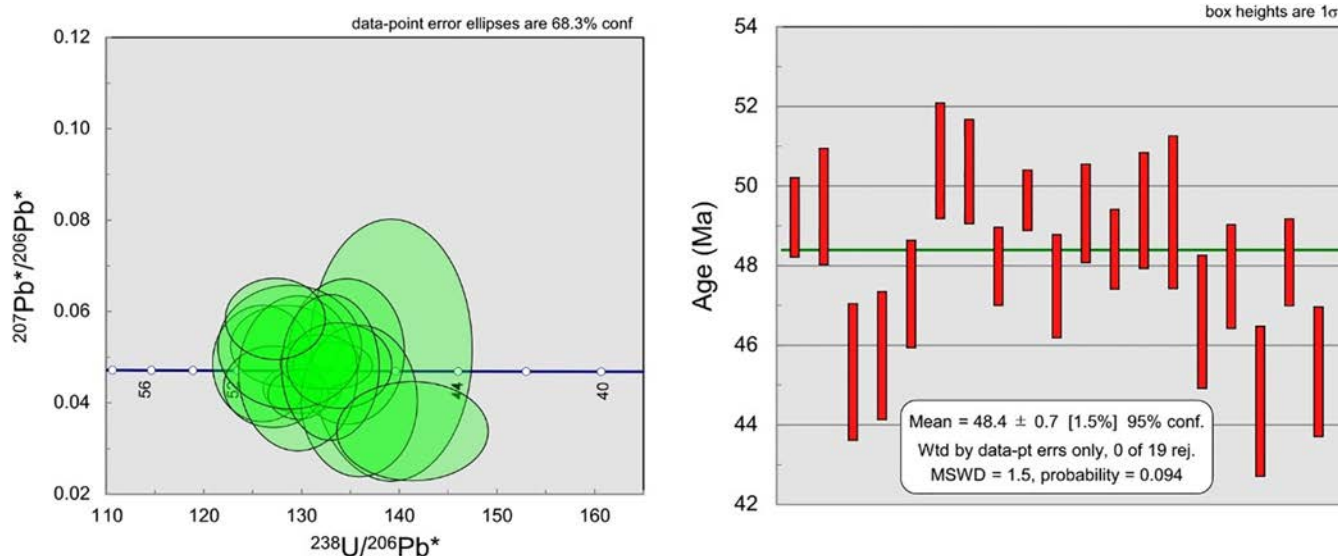
FIGURE 12 Terra–Wasserburg concordia diagram and distribution of zircon U–Pb ages for adakite of sample SE4141A processed at the National Museum of Nature and Science, Japan

210–280 Ma, Ar–Ar hornblende age of the layered gabbro (B1, this study). In general, the dyke rocks of Suite A are Cretaceous–Paleogene in age, whereas those of Suite B are Permian–Triassic. This may reflect a major change in magma sources, as we discuss later.

4 | DISCUSSION

4.1 | Origin of Suite A

As shown in most of the classical Harker and Sr/Y–La/Yb diagrams (Figure 8), the present data for dolerites, picrites, and basalts of Suite A are plotted in the domain/trend of ordinary arc rocks with adakitic variations. These trends probably represent the conventional "ordinary arc" magma sourced from the mantle wedge with some contribution from adakitic (slab-derived) melts and the crustal contamination (Castillo, 2012; Moyen, 2009; Wu et al., 2017). The ratios of Th/Yb versus Ta/Yb, Ba/Yb versus Th/Yb, and Nb/Y versus Zr/Y (Figure 14; Condie, 2005; Pearce, 1983; Pearce et al., 2005; Pearce & Reagan, 2019) indicate that the rocks of Suite A are mostly calc-alkaline, probably originated along an active continental margin with an enriched mantle wedge underneath. In addition, the parent magmas were influenced by melts/fluids ascending from both shallower and deeper parts of the subducting slab reflected by higher Ba/Yb and Th/Yb ratios, respectively (Figure 14d; Pearce et al., 2005). No significant contribution from the depleted mantle is detected (Figure 14b,c).

Petrology of the adakitic rocks from Primorye was recently described in detail by Wu et al. (2017). Their study concluded that the Cretaceous adakites had originated from the partial melting of meta-mafic rocks from the subducted slab. In contrast, the Eocene adakitic rocks were likely derived from subduction-related andesitic melts that underwent fractionation of clinopyoxene, orthopyroxene, garnet and amphibole. However, the Sr–Nd isotopic data of this study show that the Eocene adakites might have also been strongly influenced by metabasalts of subducted slab (Figure 11).

4.2 | Origin of Suite B

In contrast to the above-mentioned rocks of Suite A, gabbro, dolerite and picrite of Suite B recorded a distinct influence from a primitive/depleted mantle, indicated by the lower Ta/Yb, Nb/Y and Zr Y ratios (Figure 14b,c). These indications appear contrary to the Sr–Nd isotope systematic that suggest their geochemical similarity to an EM2 end-member of mantle rocks (Figure 11). This contradiction, nonetheless, can be explained by the hydrothermal alteration that can increase $^{87}Sr/^{86}Sr$ ratio without significant changes in Ta/Yb, Nb/Y and Zr Y ratios. The higher Ba/Yb ratio reflects shallow-subduction (Figure 14d; Pearce et al., 2005).

The rocks of Suite B also show compositional variation that is uncommon for ordinary calc-alkaline magmas; that is, anomalously high-magnesium to relatively high-aluminum compositions (Figure 8). A similar trend was reported from the Recent basalt lavas in the Aleutian Arc (Gust & Perfit, 1987), and also from the primitive high-Mg basaltic dykes (associated with high-Al basalt), andesite, and dacite intruded into the Paleogene Adamello Batholith in the European Alps (Figure 15a; Hürlimann et al., 2016). The relevant petrological experiments showed that the Adamello high-Mg basalts had generated from partial melts at pressure of 2.7 ± 0.2 GPa and temperature of 1390 ± 30 °C, that is, nearly in the condition of the spinel–garnet transition in mantle peridotite. On the other hand, the basaltic andesites and dacites in the same batholith were likely differentiated from mafic magmas as a result of fractional crystallization at mid- to deep-crustal levels. The trace element chemistry of amphiboles from the andesite
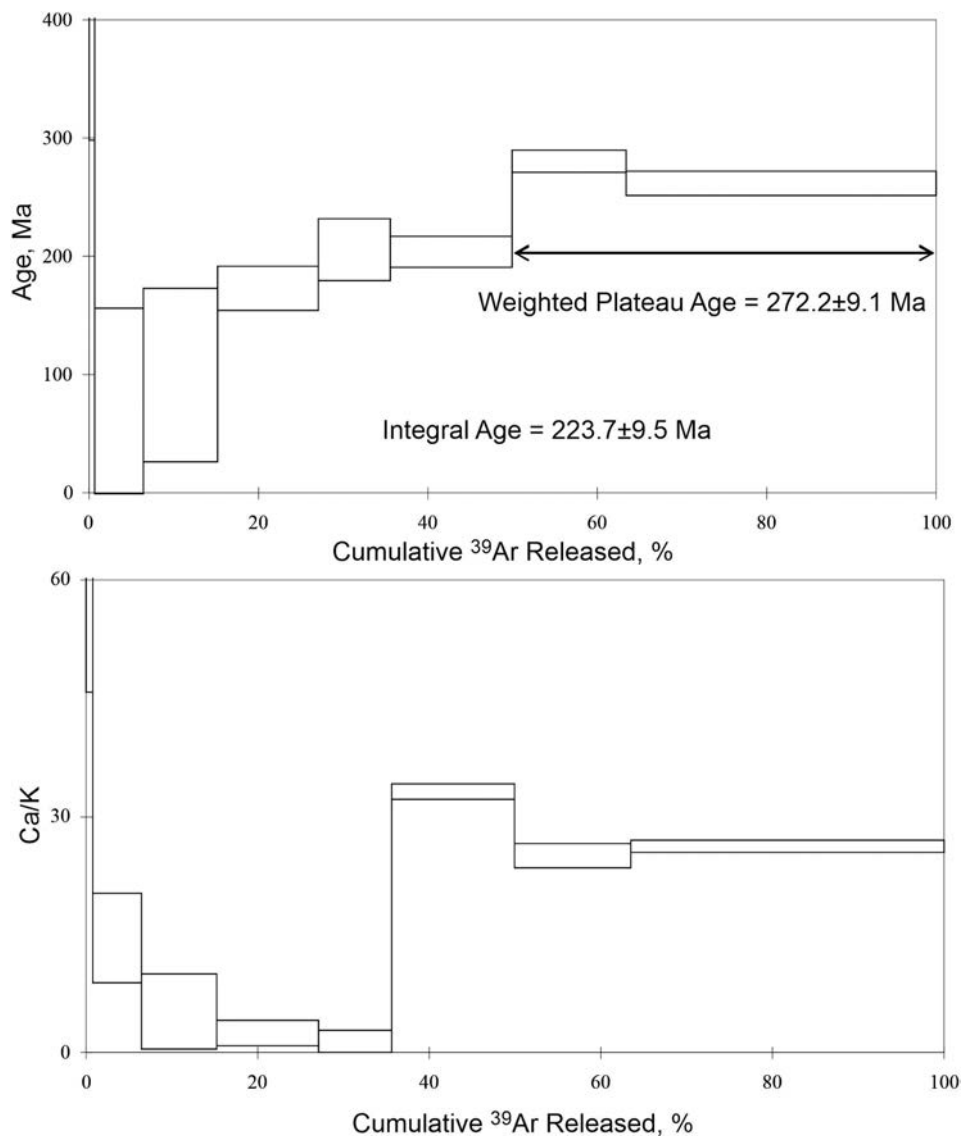
dykes revealed the coexistence of amphibole with the primitive melts that indicates elevated H_2O contents in their parental magmas (Hürlimann et al., 2016).

According to Schmidt and Jagoutz (2017), the generation of an extremely high-Mg melt (MgO > 14 wt.% at SiO_2 = 42–50 wt.%) in the arc environments is globally rare. For making such a melt, high temperature and significant fluid contribution are inevitable; nonetheless, these may occur in subduction systems polluted by mantle plume. This notion is supported by the recent petrological experiments and review on widely ranging geochemical data for actual arc lavas by Pearce and Reagan (2019). Figure 14b shows that the Th/Yb and Ta/Yb ratios of the B1-type gabbros (this study) are similar to those of the plume-sourced rocks, as they are plotted along the plume-subduction interaction trend of Pearce and Reagan (2019). Their experiments also showed that anhydrous clinopyroxene-saturated melting of depleted mantle might produce high-Mg picritic magmas similar to the B1-type rocks of this study (Figure 15b). The presence of abundant hornblende in the gabbros of Suite B disprove

the generation of anhydrous melting. At the same time, the primitive high-Mg melts suggested by Hürlimann et al. (2016) may explain the appearance of the B1-type magma in a water-rich arc environment. Summarizing the above discussion, we suppose that the high-Mg rocks of B1-type have been generated from the hydrous partial melting in a plume-influenced shallow-subduction setting.

4.3 | Hybrid origin of Cr-spinel

Figure 16 shows a wide compositional variation in Cr-spinel that is abundant in some high-Mg varieties of Suite B and also common in associated high-Al rocks and the A4-type andesite. Cr-spinel in the B1 and B2-type mafic rocks are plotted in the domains ranging from the oceanic-island (OIB, plume-related) and back-arc (BABB-MORB) to arc settings, whereas those in the A4-type andesite are strictly in the arc setting. The association in the studied rocks of these two types (plume- and arc-related) of Cr-spinel is explained accordingly by the plume-
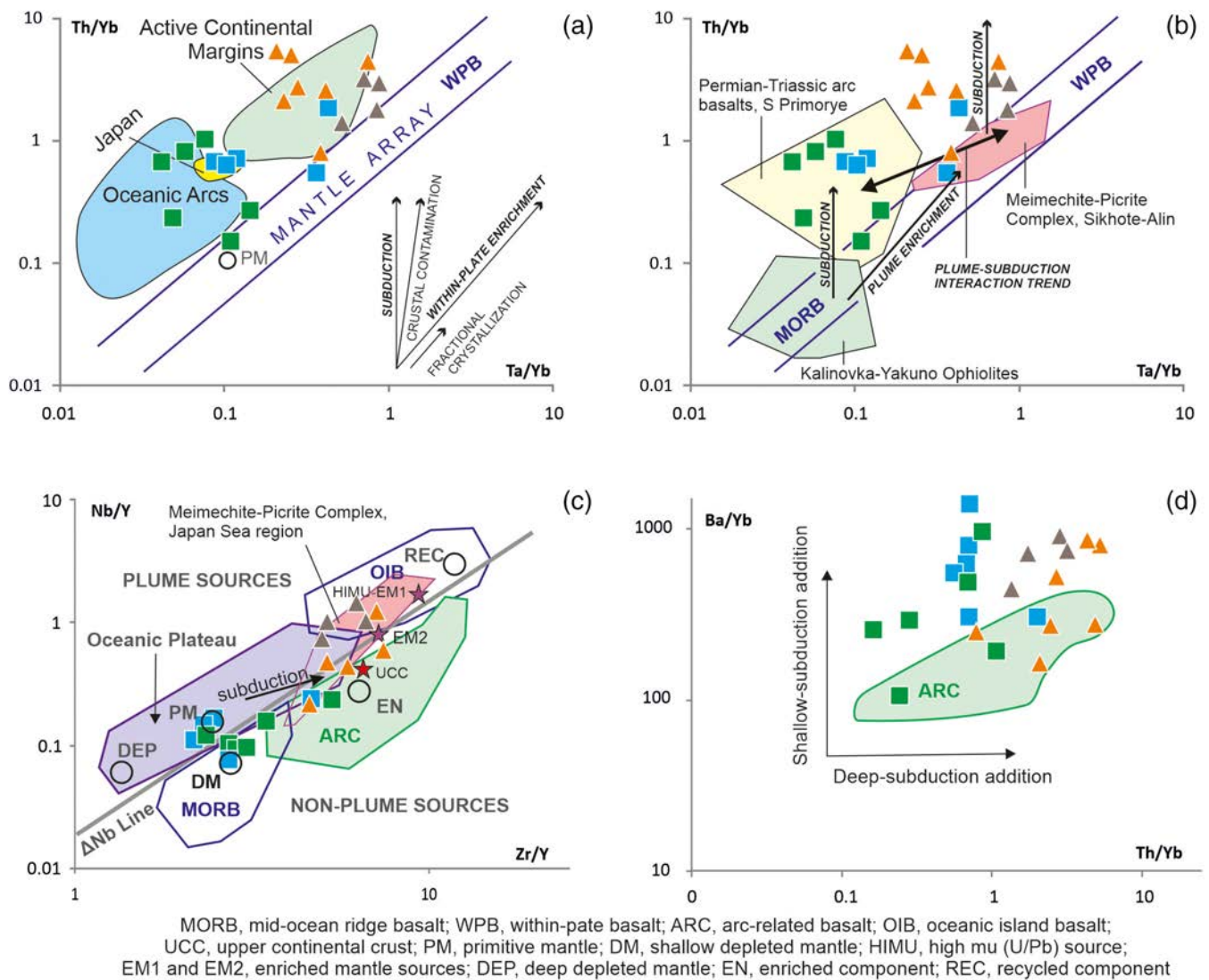
FIGURE 14 Th/Yb versus Ta/Yb (Pearce, 1983), Ba/Yb versus Th/Yb (Pearce et al., 2005), and Nb/Y versus Zr/Y (Condie, 2005) diagrams for the studied mafic rocks. (b, c) Show the Permian-earliest Cretaceous mafic rocks from different areas of the Primorye region (Chashchin et al., 2020; Golozubov et al., 2017; Ichiyama & Ishiwatari, 2004; Ishiwatari, 1985; Khanchuk & Vysotskiy, 2016; Kruk et al., 2016; Kutsukake et al., 2010; Prikhod'ko & Petukhova, 2011). In addition, unpublished data by N. N. Kruk on the Permian–Triassic volcanic rocks from the studied area and the areas of Vladivostok and Barabash cities (the Dunay, Barabash, and Vladivostok formations, respectively) are used to outline the field for Permian–Triassic arc basalts from South Primorye. See Figure 8 for symbols

subduction interaction suggested above. A few spinel grains from the B2- and A4-type rocks with compositions that do not correspond to any of the mentioned geodynamic settings may reflect some alteration.

The diagrams of Figure 16 also demonstrate that Cr-spinels from the Permian–Triassic Kalinovka and Yakuno Ophiolites in southern Primorye and Japan (Figure 1) generally indicate a MORB-type (DMM, depleted mantle) source, whereas those from the Jurassic-earliest Cretaceous Meimechite–Picrite Complex indicate an OIB source possibly related to a mantle plume (Ishiwatari & Ichiyama, 2004; Prikhod'ko & Petukhova, 2011; Simonov et al., 2014). In addition, Cr spinels from all the rocks under consideration, that is, those from the rocks of the B1-, B2-,and A4-types and the Kalinovka and Yakuno Ophiolites, share similar geochemical characteristics, suggesting their

genetic relations; for example, the formation within the same arc and back-arc settings thoroughly influenced by a mantle plume activity.

4.4 | Major change in magma sources

The geochemical characteristics of small-scale mafic intrusions and lavas around the Sea-of-Japan region is summarized in diagram of Figure 14b, in which all the analyzed dyke rocks from the Sergeevka belt are plotted in the domain of subduction-related magmas. In contrast, the ophiolite and meimechite–picrite complexes from the same region are plotted almost totally in the domain suggesting mantle-plume origin.
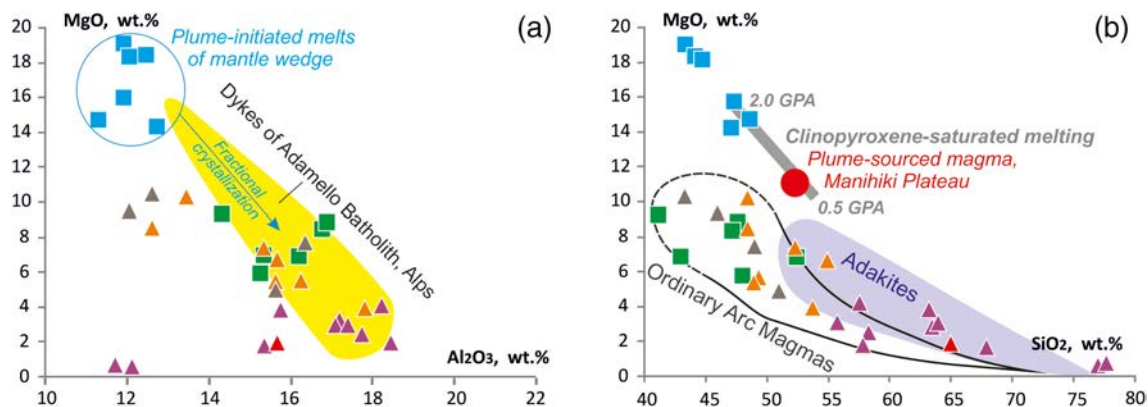
FIGURE 15 MgO versus Al$_2$O$_3$ and SiO$_2$ for the studied rocks. Also shown are: (a) the primitive basalt-andesite-dacite dyke suite of the Adamello Batholith in the Alps (Hürlimann et al., 2016); and (b) plume-sourced magma and results of experimental melting from Pearce and Reagan (2019). Note that most rocks of meimechite–picrite complex in the Japan-Sea region have contents of MgO higher than 20 wt.% and, Al$_2$O$_3$ lower than 10 wt.%, so that their plots are positioned outside the diagram ranges. See Figure 8 for symbols

FIGURE 16 TiO$_2$ versus Cr/(Cr + Al) and Al$_2$O$_3$ diagrams by Arai (1992) and Lenaz and Princivalle (2005), respectively, for the analyzed Cr-spinel crystals for the investigated rocks from Primorye. Crystals from mafic rocks from the Kalinovka Ophiolite (Khanchuk & Vysotskiy, 2016), Yakuno Ophiolite (Ishiwatari, 1985), and meimechite–picrite complex (Shcheka, 1983; Shcheka et al., 2003, 2009; Simonov et al., 2014) from the Sikhote-Alin accretionary prism are shown for comparison
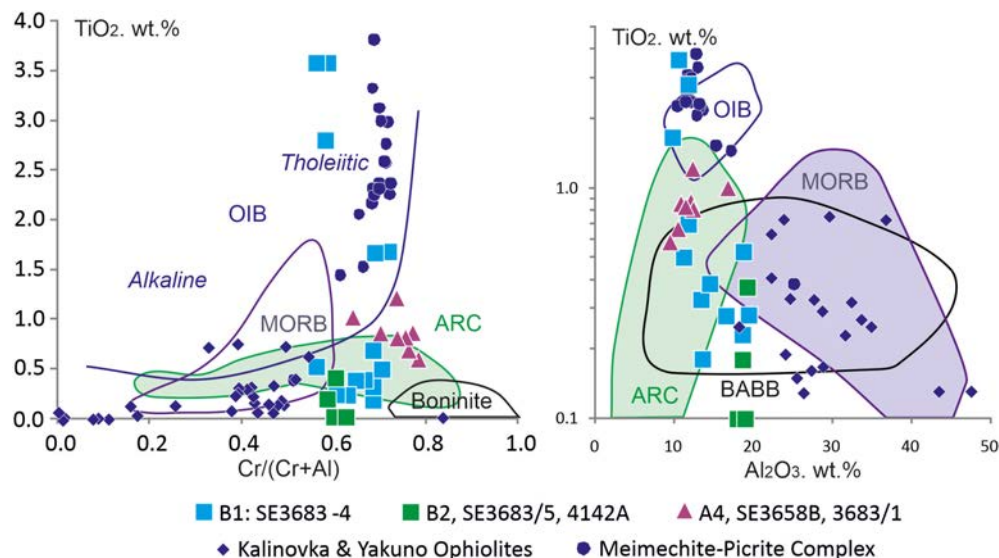
Furthermore, dyke rocks of Suite B are geochemically closer not only to the Permian–Triassic arc volcanic rocks from the southern Pimorye but also to rocks of the Kalinovka and Yakuno ophiolites from Sikhote-Alin and Japan (Figure 1). On the other hand, the rocks of Suite A are closer to the Jurassic-earliest Cretaceous meymechites and picrites in Sikhote-Alin. This contrast probably indicates that a major change in magma source occurred in southern Primorye before the Miocene opening of the Sea of Japan. Namely, the Permian–Triassic dykes were fed from a primitive/depleted mantle, whereas the early-middle Cretaceous and Paleogene dykes from an enriched (EM2) mantle (Figure 14b,c). The Jurassic-earliest Cretaceous (159–132 Ma) Meimechite-Picrite Complex has distinct signatures of mantle plume (Ishiwatari & Ichiyama, 2004; Prikhod'ko & Petukhova, 2011; Simonov et al., 2014; Figures 14b and 16), suggesting that the circum-Sea-of-Japan region was regionally affected by a plume to induce a transition in magma characters from a primitive to a more enriched composition.

The present data from southern Primorye confirm that the circum-Sea-of-Japan region has been magmatically uniform in a subduction-related regime since the Permian at least until the Paleogene, except for the Jurassic-earliest Cretaceous time when a plume activity became dominant. As the concordant results were reported also from the coeval volcanic rocks from the other side of Sea of Japan, we can conclude that this secular change is not of local but of regional context as to the circum-Sea-of-Japan domain over 2000 km in diameter.

The available dataset for mafic intrusions around the Sea-of-Japan is still too limited, but we can roughly reconstruct the secular change in magmatism as follows.

1. The initial plume-subduction interaction onset likely in the Late Permian when the angle of subducting slab became shallower; shallow enough to allow further ascent of a plume head to generate the unique magmas for the gabbro-dolerite of Suite B and the Kalinovka–Yakuno ophiolites.

2. During the Jurassic–earliest Cretaceous, the plume activity culminated, as recorded by the meimechite–picrite complex and plume-related basalts and picrites from the accretionary complexes of Central Asia, Russian Far East, and Japan (Ishiwatari et al., 2013; Ishiwatari & Ichiyama, 2004; Safonova et al., 2009; and references therein). The plume activity effectively slowed down the subduction rate throughout East Asia.

3. In the early-middle Cretaceous, as the plume activity declined, the subduction angle and rate returned to the previous status, which left the A4-type adakites.

4.5 | Tectonic implications

In this regard, the popular model of strike-slip margin for the Cretaceous East Asia (e.g., Golozoubov, 2006; Khanchuk et al., 1996, 1997, 2016, 2019; Li et al., 2020; Liu et al., 2017; Maruyama et al., 1997; Yamakita & Otoh, 2000) appears significantly discordant to the regional magmatic history discussed above. There are several key issues to be checked to prove or disprove the claimed strike-slip motion particularly during the mid-Cretaceous time. First, as to the timing, many researchers pointed out that the Albian-Cenomanian

was the time for the maximum transform motion (e.g., Khanchuk et al., 2019); however, this time interval is characterized by the above-mentioned intensive subduction-related magmatism in a regional extent. Second, magmatism in any form is less common along major strike-slip faults including transform plate boundaries (Duarte, 2019). Apparently clear NNE–SSW-running lineaments observed in Primorye and northeast China (e. g., Central Sikhote Alin fault, etc. in Figure 1) are eye-catching; nonetheless, they do not automatically indicate the claimed long-distance displacement over 1000 km, without practically testable reference points for off-set by fault. Further documentation is necessarily for confirming the real amount of displacement for each lineament.

Despite the strike-slip margin interpretation, there is a new model proposed for the East Asian margin; that is, Greater South China (GSC) (Isozaki, 2019; Isozaki et al., 2014). The reconstructed older mega-continental block named GSC includes modern-day South China block proper on the main continent, East China Sea, southwest/northeast Japan, and the Khanka/Jiamusi/Bureya megablock in Primorye/northeast China (Figure 17). This reconstruction was based on several lines of evidence; that is, the common age spectra of detrital zircons in Paleozoic sandstones reflecting the same provenance (Isozaki et al., 2014, 2015, 2017), common marine fauna for
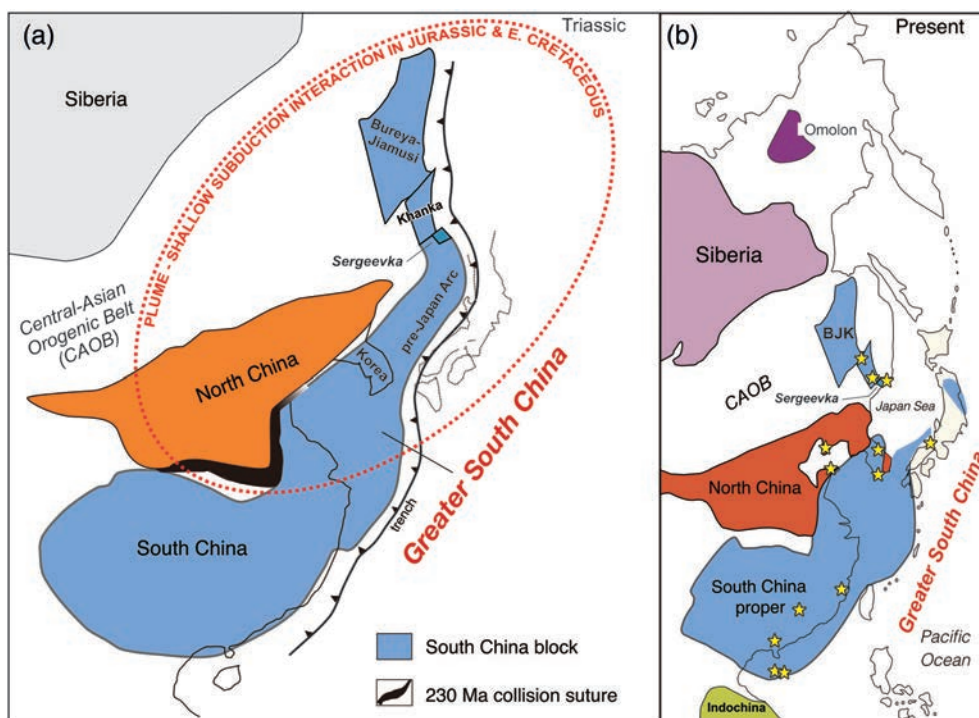

FIGURE 17 Geodynamic schemes (modified from Isozaki et al., 2017) illustrating the discussion above. (a) Paleogeographic map showing the reconstructed greater South China that includes the Khanka and Bureya-Jiamusi blocks (BJK), in a larger framework of East Asia prior to the final closure of Central-Asian Orogenic Belt and during the initial stage of East Asia plume activity. The plume-shallow subduction area is shown after the East Asian large adakitic province (Nechaev et al., 2018). (b) The current distribution of fragments of Greater South China in the East Asian region (for comparison). The yellow stars indicate locations of the Triassic mafic igneous activity after Tang et al. (2013), Wang et al. (2013), Gao et al. (2017), and Xu et al. (2018) for South China; Yang and Wu (2009) for the eastern North China; Kim and Turek (1996) and Yi et al. (2016) for Korea; Ishiwatari (1985) and Ichiyama and Ishiwatari (2004) for Japan; Golozubov et al. (2017) and Wang et al. (2015) for Khanka Massif and this study for Sergeevka belt. Note that the Jurassic and Early Cretaceous igneous activity including small mafic intrusions and lavas was more widespread, covering a large part of intracontinental East Asia (Figure 17a; Wu et al., 2005; Nechaev et al., 2018)

paleolatitude/environments in southern Primorye, northeast–southwest Japan, and South China proper (Isozaki, 2019; Zakharov et al., 1996).

In this tectonic framework, the regional occurrence of similar intrusions and lavas and their coeval shift in magmatic nature ubiquitously around the Sea of Japan (Figure 17) can be reasonably explained without assuming imaginary strike-slip dislocation. This model is supported also by other study results (Liu et al., 2017; Tsutsumi et al., 2016; Xing et al., 2019) that confirmed a significant age cluster about 500 Ma in detrital zircon that well corresponds to the ages of detrital monazite from the Cenozoic sands, and to those of zircons from the Neoproterozoic sandstones and igneous-metamorphic rocks of South China (Gao et al., 2020; Yokoyama et al., 2010).

5 | CONCLUSIONS

The present geochemical and geochronological analyses revealed that the dykes penetrated the western Sergeevka block in the southern coastal areas of Primorye are grouped into two geochemically distinct suites; that is, Suite A composed of Paleogene and Early Cretaceous adakitic and mafic rocks and Suite B of extremely high-Mg and high-Al gabbro-dolerites. Although both suites were formed within the tectonic framework of subduction from the Pacific side; Suite B is unique in recording a rare magmatic arc phenomenon. The dykes of Suite B, which are characterized geochemically by high Ba/Yb and low Nb/Y, Zr/Y, and Th/Yb ratios, were likely derived from primitive melts of mantle wedge under shallow-angle subduction setting coupled with deep mantle plume.

The Sr–Nd isotopic data further support that the magmas for intrusions were sourced both from depleted and enriched parts of mantle, that is, MORB and EM2. The Ar–Ar age for amphiboles in high-Mg gabbros indicates that this suite formed during the Permian to Late Triassic time. These Permian–Triassic mafic dykes of Suite B are geochemically close to those of the Kalinovka (Sikhote Alin)-Yakuno (southwest Japan) ophiolites in both sides of the Sea of Japan, thus they probably shared regionally the initial stage of the plume-subduction interaction along the Permo–Triassic arc. Subsequently, the meimechite–picrite complex in Sikhote-Alin, likely recorded the peak plume activity during Jurassic and earliest Cretaceous.

The adakitic and mafic rocks of the Late Cretaceous to Paleogene of Suite A likely represent magmatic records of a waning stage of the plume activity associated with deepening and accelerating subduction. In summary, the present study positively suggests a plume-related change of the mantle composition during the Jurassic-early Cretaceous (Nechaev et al., 2018); that is, from a primitive mantle to EM2, with respect to a change in subduction regime, from deep-angle during the Permian–Triassic to shallow-angle during the Triassic to Early Cretaceous, then back to deep-angle again in the mid-Cretaceous to Paleogene. The above conclusions with relevant tectono-magmatic interpretations in southern Primorye appear consistent with the data from the circum-Sea of Japan region, for example, NW China, Korean peninsula, and southwest/northeast Japan (Figure 17); on the contrary, they are significantly inconsistent with the widely accepted tectonic views of large-scale strike-slip tectonics in the early to mid-Cretaceous East Asia (e. g., Khanchuk et al., 1996, Khanchuk et al., 1997, Khanchuk et al., 2016, Khanchuk et al., 2019; Maruyama et al., 1997; Yamakita & Otoh, 2000; Golozoubov, 2006; Liu et al., 2017; Li et al., 2020). Instead, the recent-proposed tectonic framework of GSC (Isozaki, 2019; Isozaki et al., 2014, 2015; Isozaki et al., 2017) appears more suitable for all available data on the Late Paleozoic to Paleogene magmatism in the circum-Sea of Japan region in Far East Asia.

ORCID

Victor P. Nechaev https://orcid.org/0000-0002-6229-5495
Evgene V. Sklyarov https://orcid.org/0000-0002-9194-5506
Yukio Isozaki https://orcid.org/0000-0002-3596-581X
Nikolay N. Kruk https://orcid.org/0000-0003-4166-1000
Alexey V. Travin https://orcid.org/0000-0002-5640-4560
Yukiyasu Tsutsumi https://orcid.org/0000-0001-9593-0822
Eugenia V. Nechaeva https://orcid.org/0000-0002-3858-1627

REFERENCES

Arai, S. (1992). Chemistry of chromian spinel in volcanic rocks as a potential guide to magma chemistry. *Mineralogical Magazine, 56,* 173–184.

Baksi, A. K., Archibald, D. A., & Farrar, E. (1996). Intercalibration of $^{40}Ar/^{39}Ar$ dating standards. *Chemical Geology, 129,* 307–324.

Castillo, P. R. (2012). Adakite petrogenesis. *Lithos, 135,* 304–316.

Chashchin, A. A., Chashchin, S. A., Kasatkin, S. A., & Golozubov, V. V. (2020). Late Triassic volcanic rocks of Talminsky complex (southwestern Primorye): Mineralogy, geochemistry and genesis. *Modern Problems of Science and Education, 11,* 139–148.

Chashchin, A., Nechaev, V., Nechaeva, E., & Blokhin, M. (2011). Discovery of Eocene adakites in Primor'e. *Doklady Earth Sciences, 438*(2), 744–749.

Condie, K. C. (2005). High field strength element ratios in Archean basalts: A window to evolving sources of mantle plumes? *Lithos, 79,* 491–504.

Davis, G. A. (2003). The Yanshan belt of North China: Tectonics, adakitic magmatism, and crustal evolution. *Earth Science Frontiers, 10*(4), 373–384.

Duarte, J. C. (Ed.). (2019). *Transform plate boundaries and fracture zones* (1st ed., p. 478). Elsevier.

Ewart, A. (1982). The mineralogy and petrology of tertiary-recent orogenic volcanic rocks: With special reference to the andesitic-basaltic compositional range. In R. S. Thorpe (Ed.), *Andesites: Orogenic andesites and related rocks* (pp. 25–98). Wiley.

Fleck, R. J., Sutter, J. F., & Elliot, D. H. (1977). Interpretation of discordant 40Ar/39Ar age-spectra of mesozoic tholeiites from Antarctica. *Geochimica et Cosmochimica Acta, 41*(1), 15–32.

Ganbat, A., Tsujimori, T., Miao, L.-C., Safonova, I., Pastor-Galán, D., Anaad, C., Baatar, M., Aoki, S., Aoki, K., & Savinskiy, L. (2021). Late Paleozoic–Early Mesozoic granitoids in the Khangay–Khentey basin, Central Mongolia: Implication for the tectonic evolution of the Mongol–Okhotsk Ocean margin. *Lithos*, 404-405, 106455. https://doi.org/10.1016/j.lithos.2021.106455

Gao, F., Pei, X., Li, R., Li, Z., Pei, L., Chen, Y., Wang, M., Zhao, S., Liu, C., & Li, X. (2020). Neoproterozoic tectonic evolution of the northwestern margin of the Yangtze Block (southwestern China): Evidence from sandstone geochemistry and detrital zircon U-Pb ages of the Hengdan Group. *Precambrian Research*, 344, 105737.

Gao, P., Zheng, Y. -F., & Zhao, Z. -F. (2017). Triassic granites in South China: A geochemical perspective on their characteristics, petrogenesis, and tectonic significance. *Earth-Science Reviews*, 173, 266–294.

Golozoubov, V. V. (2006). *Tectonics of the Jurassic and Lower Cretaceous complexes of the north-western framing of the Pacific Ocean* (p. 239). Dal'nauka (in Russian).

Golozoubov, V. V., & Khanchuk, A. I. (2011). Tectonics of Sergeevka Terrane (Southern Sikhote-Alin). In *Field guide* (p. 11). Dal'nauka (in Russian).

Golozoubov, V. V., Markevich, V. S., & Bugdaeva, E. V. (1999). Early Cretaceous changes of vegetation and environment in East Asia. *Palaeogeography, Palaeoclimatology, Palaeoecology*, 153(1–4), 139–146.

Golozubov, V. V., Kruk, N. N., Kiselyov, V. I., Rudnev, S. N., Kasatkin, S. A., & Kruk, E. A. (2017). First evidence for the Middle Triassic volcanism in South Primorye. *Russian Journal of Pacific Geology*, 11(2), 110–122.

Gonevchuk, V. G., Gonevchuk, G. A., Sayadyan, G. R., & Seltman, P. (1999). REE in the tin- and gold-bearing granitoids of Sikhote-Alin as indicators of their genesis. In A. I. Khanchuk (Ed.), *Geodynamics and metallogeny* (pp. 109–111). Dal'nauka (in Russian).

Govorov, I. N., Blagodareva, N. S., & Zhuravlev, D. Z. (1997). Petrogenesis of fluorite deposits of the Voznesensky district (Primorye) from the data of Rb-Sr isotopy of magmatic and metasomatic rocks. *Tikhookeanskaya Geologiya*, 16(5), 60–69 (in Russian).

Grebennikov, A. V., Khanchuk, A. I., Gonevchuk, V. G., & Kovalenko, S. V. (2016). Cretaceous and Paleogene granitoid suites of the Sikhote-Alin area (Far East Russia): Geochemistry and tectonic implications. *Lithos*, 261, 250–261.

Guo, F., Nakamura, E., Fan, W., Kobayashi, K., Li, C., & Gao, X. (2009). Mineralogical and geochemical constraints on magmatic evolution of Paleocene adakitic andesites from the Yanji area, NE China. *Lithos*, 112(3–4), 321–341.

Guo, F., Nakamura, E., Fan, W. M., Kobayashi, K., & Li, C. W. (2007). Generation of Palaeocene adakitic andesites by magma mixing; Yanji area, NE China. *Journal of Petrology*, 46, 661–692.

Gust, D. A., & Perfit, M. R. (1987). Phase relations of a high-Mg basalt from the Aleutian Island Arc: Implications for primary Island arc basalts and high-Al basalts. *Contributions to Mineralogy and Petrology*, 97, 7–18.

Hart, S. R. (1988). Heterogeneous mantle domains: Signatures, genesis and mixing chronologies. *Earth and Planetary Science Letters*, 90(3), 273–296.

Hürlimann, N., Müntener, O., Ulmer, P., Nandedkar, R., Chiaradia, M., & Ovtcharova, M. (2016). Primary magmas in continental arcs and their differentiated products: Petrology of a post-plutonic dyke suite in the Tertiary Adamello Batholith (Alps). *Journal of Petrology*, 57(3), 495–534.

Ichiyama, Y., & Ishiwatari, A. (2004). Petrochemical evidence for off-ridge magmatism in a back-arc setting from the Yakuno ophiolite, Japan. *The Island Arc*, 13(1), 157–177.

Imaoka, T., Kawabata, H., Nagashima, M., Nakashima, K., Kamei, A., Yagi, K., Itaya, T., & Kiji, M. (2017). Petrogenesis of an early Cretaceous lamprophyre dike from Kyoto Prefecture, Japan: Implications for the generation of high-Nb basalt magmas in subduction zones. *Lithos*, 290-291, 18–33.

Ishiwatari, A. (1985). Igneous petrogenesis of the Yakuno ophiolite (Japan) in the context of the diversity of ophiolites. *Contributions to Mineralogy and Petrology*, 89, 155–167.

Ishiwatari, A., & Tsujimori, T. (2003). Paleozoic ophiolites and blueschists in Japan and Russian Primorye in the tectonic framework of East Asia: A synthesis. *The Island Arc*, 12, 190–206.

Ishiwatari, A., & Ichiyama, Y. (2004). Alaskan-type plutons and ultramafic lavas in Far East Russia, Northeast China, and Japan. *International Geology Review*, 46, 316–331.

Ishiwatari, A., Ichiyama, Y., & Ganbat, E. (2013). Plume type ophiolites in Japan, East Russia and Mongolia: Peculiarity of the Late Jurassic examples. *Geophysical Research Abstracts*, 15, EGU2013-13609.

Isozaki, Y. (2019). A visage of early Paleozoic Japan: Geotectonic and paleobiogeographical significance of Greater South China. *Island Arc*, 28(3), e12296.

Isozaki, Y., Aoki, K., Sakata, S., & Hirata, T. (2014). The eastern extension of Paleozoic South China in NE Japan evidenced by detrital zircon U-Pb ages. *GFF*, 136, 116–119 (original proposal of GSC).

Isozaki, Y., Ehiro, M., Nakahata, H., Aoki, K., Sakata, S., & Hirata, T. (2015). Cambrian arc plutonism in Northeast Japan and its significance in East Asia: New U-Pb zircon ages of the oldest granitoids in the Kitakami and Ou Mountains. *Journal of Asian Earth Sciences*, 108, 136–149.

Isozaki, Y., Nakahata, H., Zakharov, Y. D., Popov, A. M., Sakata, S., & Hirata, T. (2017). Greater South China extended to the Khanka block: Detrital zircon chronology of the middle-upper Paleozoic sandstones of the Sergeevka belt, Far East Russia. *Journal of Asian Earth Sciences*, 145, 565–575.

Ivanov, A. V., Mukasa, S. B., Kamenetsky, V. S., Ackerson, M., Demonterova, E. I., Pokrovsky, B. G., Vladykin, N. V., Kolesnichenko, M. V., Litasov, K. D., & Zedgenizov, D. A. (2018). Volatile concentrations in olivine-hosted melt inclusions from meimechite and melanephelinite lavas of the Siberian Traps Large Igneous Province: Evidence for flux-related high-Ti, high-Mg magmatism. *Chemical Geology*, 483, 442–462.

Jacobsen, S. B., & Wasserburg, G. J. (1980). Sm-Nd isotopic evolution of chondrites. *Earth and Planetary Science Letters*, 50, 139–155.

Jahn, B. -M., Valui, G., Kruk, N., Gonevchuk, V., Usuki, M., & Wu, J. T. J. (2015). Emplacement ages, geochemical and Sr–Nd–Hf isotopic characterization of Mesozoic to early Cenozoic granitoids of the Sikhote-Alin Orogenic Belt, Russian Far East: Crustal growth and regional tectonic evolution. *Journal of Asian Earth Sciences*, 111, 872–918. https://doi.org/10.1016/j.jseaes.2015.08.012

Ji, W., Xu, W., Yang, D., Pei, F., Jin, K., & Liu, X. (2007). Chronology and geochemistry of volcanic rocks in the Cretaceous Suifenhe formation in eastern Heilongjiang, China. *Acta Geologica Sinica*, 81(2), 266–277.

Kemkin, I. V., & Khanchuk, A. I. (1993). Jurassic accretionary complex of Sikhote-Alin. *Tikhookeanskaya Geologiya*, 5, 31–42 (in Russian).

Kemkin, I. V., Kametaka, M., & Kojima, S. (1999). Radiolarian biostratigraphy for transitional facies of chert-clastic sequence of the Taukha terrane in the Koreyskaya River area, Southern Sikhote-Alin, Russia. *Journal of Earth and Planetary Sciences, Nagoya University*, 46, 29–47.

Kemkin, I. V., Rudenko, V. S., & Taketani, Y. (1997). Some Jurassic and Early Cretaceous radiolarians from chert-terrigenous sequence of the Taukha Terrane, southern Sikhote-Alin. *Memories of the Geological Society of Japan*, 48, 163–175.

Khanchuk, A. I. (2001). Pre-Neogene tectonics of the Sea-of-Japan region: A view from the Russian side. *Earth Science (Chikyu Kagaku)*, 55, 275–291.

Khanchuk, A. I., & Vysotskiy, S. V. (2016). Different-depth gabbro–ultrabasite associations in the Sikhote-Alin ophiolites (Russian Far East). *Russian Geology and Geophysics*, 57(1), 141–154.

Khanchuk, A. I., Golozubov, V. V., Martynov Yu, A., & Simanenko, V. P. (1997). Early Cretaceous and Paleogene transform continental margins (Californian type) of the Russian Far East. In Y. V. Karyakin (Ed.), *Tectonics of Asia* (pp. 240–243). GEOS (in Russian).

Khanchuk, A. I., Grebennikov, A. V., & Ivanov, V. V. (2019). Albian–Cenomanian orogenic belt and igneous province of Pacific Asia. *Russian Journal of Pacific Geology*, 13, 187–219.

Khanchuk, A. I., Kemkin, I. V., & Kruk, N. N. (2016). The Sikhote-Alin orogenic belt, Russian South East: Terranes and the formation of continental lithosphere based on geological and isotopic data. *Journal of Asian Earth Sciences*, 120, 117–138.

Khanchuk, A. I., Ratkin, V. V., Ryazantseva, M. D., Golozubov, V. V., & Gonokhova, N. G. (1996). *Geology and mineral deposits of Primorskiy Krai* (p. 61). Dal'nauka.

Kim, C. B., & Turek, A. (1996). Advances in U-Pb zircon geochronology of Mesozoic plutonism in the southwestern part of Ryeongnam massif, Korea. *Geochemical Journal*, 30, 323–338.

Kim, J. S., Son, M., Kim, J. S., & Kim, J. (2005). $^{40}Ar/^{39}Ar$ ages of the Tertiary dike swarm and volcanic rocks, SE Korea. *The Journal of the Petrological Society of Korea*, 14, 93–107 (in Korean with English abstract).

Kogan, B. S. (1976). Phlogopite camptonite of Primorye. *Izvestiya AN SSSR, Seriya Geologicheskaya*, 1, 139–143 (in Russian).

Kojima, S., Kemkin, I. V., Kametaka, M., & Ando, A. (2000). A correlation of accretionary complexes of southern Sikhote-Alin of Russia and the inner zone of Southwest Japan. *Geosciences Journal*, 4(3), 175–185.

Kruk, N. N., Golozoubov, V. V., Khanchuk, A. I., Aleksandrov, I. A., Chashchin, A. A., & Sklyarov, E. V. (2018). *Intrusive complexes of Sergeevka Terrane—The oldest block of South Primorye* (p. 55). Dal'nauka (in Russian).

Kruk, N. N., Golozubov, V. V., Kasatkin, S. A., & Kruk, E. A. (2016). Permian volcanic rocks of the Southern Primorye: Geochemistry, melt sources, and possible tectonic position. In A. I. Khanchuk (Ed.), *Geological processes in settings of subduction, collision, and transform plate margins. Proceedings of third All-Russian Conference* (pp. 184–186). Dal'nauka (in Russian).

Kruk, N. N., Golozoubov, V. V., Kiselev, V. I., Kruk, E. A., Rudnev, S. N., Serov, P. A., Kasatkin, S. A., & Moskalenko, E. Y. (2018). Paleozoic granitoids of the southern part of the Voznesenka Terrane (Southern Primorye): Age, composition, melt sources, and tectonic settings. *Russian Journal of Pacific Geology*, 12(3), 190–209.

Kutsukake, T., Nakano, S., & The Collaborative Research Group for the Granite Around Lake Biwa. (2010). Geochemistry and mineral chemistry of mafic dykes associated with Hiei pluton, Southwest Japan. *Journal of Mineralogical and Petrological Sciences*, 105, 309–319.

Le Maitre, R. W. (Ed.). (2002). *Igneous rocks: A classification and glossary of terms. Recommendations of the International Union of Geological Sciences Subcommission on the Systematics of Igneous Rocks* (p. 256). Cambridge University Press.

Lenaz, D., & Princivalle, F. (2005). Crystal chemistry of detrital Cr-spinels from SE Alps and Outer Dinarides: A new tool to discriminate supplies from different provenance areas with similar tectonic setting? *Canadian Mineralogist*, 43, 1305–1314.

Li, Y., Xu, W. -L., Zhu, R. -X., Wang, F., Ge, W. -C., & Sorokin, A. A. (2020). Late Jurassic to early Early Cretaceous tectonic nature on the NE Asian continental margin: Constraints from Mesozoic accretionary complexes. *Earth-Science Reviews*, 200, 103042.

Liu, K., Zhang, J., Wilde, S. A., Liu, S., Guo, F., Kasatkin, S. A., Golozoubov, V. V., Ge, M., Wang, M., & Wang, J. (2017). U-Pb dating and Lu-Hf isotopes of detrital zircons from the southern Sikhote-Alin orogenic belt, Russian Far East: Tectonic implications for the Early Cretaceous evolution of the Northwest Pacific margin. *Tectonics*, 36, 2555–2598.

Liu, S., Li, S., Guo, S., Hou, Z., & He, Y. (2012). The Cretaceous adakitic–basaltic–granitic magma sequence on south-eastern margin of the North China Craton: Implications for lithospheric thinning mechanism. *Lithos*, 134-135, 163–178.

Lugmair, G., & Marti, K. (1978). Lunar initial $^{143}Nd/^{144}Nd$: Differential evolution of the lunar crust and mantle. *Earth and Planetary Science Letters*, 39, 349–357.

Maksimov, S. O., & Sakhno, V. G. (2008). Geochronology of basalt volcanism on the Shufan Plateau (Primorye). *Doklady Earth Sciences*, 422(7), 1044–1049.

Malinovsky, A. I., Golozoubov, V. V., Simanenko, V. P., & Simanenko, L. F. (2008). Kema terrane: A fragment of a back-arc basin of the early Cretaceous Moneron-Samarga Island-arc system, East Sikhote-Alin range, Russian Far East. *The Island Arc*, 17(3), 285–304.

Martynov, Y. A., Golozubov, V. V., & Khanchuk, A. I. (2016). Mantle diapirism at convergent boundaries (Sea of Japan). *Russian Geology and Geophysics*, 57, 733–743.

Maruyama, S., Isozaki, Y., & Terabayashi, M. (1997). Paleogeographic maps of the Japanese Islands: Plate tectonic synthesis from 750 Ma to the present. *The Island Arc*, 6, 124–142.

McDonough, W. F., & Sun, S. -S. (1995). The composition of the Earth. *Chemical Geology*, 120, 223–253.

Mel'nikov, N. G., & Izosov, L. A. (1984). Structure-formation zoning of Primorye. *Tikhookeanskaya Geologiya*, 1, 53–61 (in Russian).

Moyen, J. -F. (2009). High Sr/Y and La/Yb ratios: The meaning of the "adakitic signature". *Lithos*, 112, 556–574.

Murphy, J. B. (2013). Appinite suites: A record of the role of water in the genesis, transport, emplacement and crystallization of magma. *Earth-Science Reviews*, 119, 35–59.

Murphy, J. B. (2019). Appinite suites and their genetic relationship with coeval voluminous granitoid batholiths. *International Geology Review*, 6, 683–713.

Nechaev, V. P., Dai, S., Sutherland, F. L., Graham, I. T., & Nechaeva, E. V. (2018). The Cretaceous turn of geological evolution: Key evidence from East Asia. *Acta Geologica Sinica*, 92(5), 1991–2003.

Nechaev, V. P., Losiv, V. M., Chekryzhov, I. Y., & Agoshkov, A. I. (2015). Hydrocarbon prospects of Mesozoic fold-thrust structures of Primorye, Far East Russia. *Tikhookeanskaya Geologiya*, 34(6), 91–101 (in Russian).

Nechaev, V. P., Markevich, P. V., Malinovsky, A. I., Philippov, A. N., & Vysotskiy, S. V. (1996). Tectonic setting of the Cretaceous sediments in the Lower Amur region, Russian Far. *Journal of Sedimentological Society of Japan*, 43, 69–81.

Nechaev, V. P., Musashino, M., & Lee, D. W. (1999). Jurassic-Lower Cretaceous geodynamic evolution of the Asian eastern margin: Reconstruction pertaining to variations in heavy mineral associations from sedimentary rocks. *Geology of Pacific Ocean*, 14, 839–856.

Nevolin, P. L., Utkin, V. P., & Mitrokhin, A. N. (2011). *Tafuinsky granite massif: Structures and dynamics of their formation (Guidebook of geologic excursion route)* (p. 46). Far East Geological Institute FEB RAS (in Russian).

Okamura, S., Arculus, R. J., & Martynov, Y. A. (2005). Cenozoic magmatism of the northeastern Eurasian margin: The role of lithosphere versus asthenosphere. *Journal of Petrology*, 46(2), 221–253.

Okamura, S., Martynov, Y. A., Furuyama, K., & Nagao, K. (1998). K-Ar ages of the basaltic rocks from Far East Russia: Constraints on the tectono-magmatism associated with the Sea-of-Japan opening. *The Island Arc*, 7, 271–282.

Osozawa, S., Usuki, T., Usuki, M., Wakabayashi, J., & Jahn, B. (2019). Trace elemental and Sr-Nd-Hf isotopic compositions, and U-Pb ages for the Kitakami adakitic plutons: Insights into interactions with the early Cretaceous TRT triple junction offshore Japan. *Journal of Asian Earth Sciences*, 184, 103968.

Panteeva, S. V., Gladkochoub, D. P., Donskaya, T. V., Markova, V. V., & Sandimirova, G. P. (2003). Determination of 24 trace elements in felsic rocks by inductively coupled plasma mass spectrometry after lithium metaborate fusion. *Spectrochimica Acta Part B: Atomic Spectroscopy*, 58(2), 341–350.

Pearce, J. A. (1983). Role of sub-continental lithosphere in magma genesis at active continental margins. In C. J. Hawkesworth & M. L. Nurry (Eds.), *Continental basalts and mantle xenoliths* (pp. 230–249). Shiva.

Pearce, J. A., & Reagan, M. K. (2019). Identification, classification, and interpretation of boninites from Anthropocene to Eoarchean using Si-Mg-Ti systematics. *Geosphere*, 15(4), 1008–1037.

Pearce, J. A., Stern, R. J., Bloomer, S. H., & Fryer, P. (2005). Geochemical mapping of the Mariana arc-basin system: Implications for the nature and distribution of subduction components. *Geochemistry Geophysics Geosystems*, 6, Q07006.

Peucat, J. J., Vidal, P., Bernard-Griffiths, J., & Condie, K. C. (1989). Sr, Nd, and Pb isotopic systematics in the Archean low-to high-grade transition zone of southern India: Synaccretion versus post-accretion granulites. *Journal of Geology*, 97, 537–549.

Pin, C., & Zalduegui, J. S. (1997). Sequential separation of light rare-earth elements, thorium and uranium by miniaturized extraction chromatography: Application to isotopic analyses of silicate rocks. *Analytica Chimica Acta*, 339(1–2), 79–89.

Podolyan, V. I., & Sedykh, A. K. (1997). Coal base of Russia. In *Coal basins and deposits of Far East Russia (Khabarovsk Krai, Amur Oblast', Primorsky Krai, Jewish Autonomous Oblast')*, Vol. V (p. 371). Geoinformmark (in Russian).

Pouclet, A., Lee, J. -S., Vidal, P., Coesens, B., & Bellon, H. (1995). Cretaceous to Cenozoic volcanism in South Korea and in the Sea of Japan: Magmatic constraints on the opening of the back-arc basin. In J. L. Smellie (Ed.), *Volcanism associated with extension at consuming plate margins* (Vol. 81, pp. 169–191). Geological Society Special Publication.

Prikhod'ko, V. S., & Petukhova, L. L. (2011). Ultramafic dykes in the Samarka accretionary complex of Sikhote-Alin. In V. A. Koroteev (Ed.), *Volcanism and geodynamics* (pp. 152–154). IGG UrO RAN (in Russian).

Safonova, I. Y., Utsunomiya, A., Kojima, S., Nakae, S., Tomurtogoo, O., Filippov, A. N., & Koizumi, K. (2009). Pacific superplume-related oceanic basalts hosted by accretionary complexes of Central Asia, Russian Far East and Japan. *Gondwana Research*, 16, 587–608.

Sayadyan, G. R., Gonevchuk, V. G., Gerasimov, N. S., & Khomich, V. G. (1996). Geological and isotopic-geochemical basis for basing the age and formation sequence of magmatic rocks of the Krinichnoye gold ore field. In S. A. Shcheka (Ed.), *Mineralogo-Geokhimicheskiye Indikatory Rudonosnosti I Petrogenezisa* (pp. 93–105). Dal'nauka (in Russian).

Schmidt, M. W., & Jagoutz, O. (2017). The global systematics of primitive arc melts. *Geochemistry Geophysics Geosystems*, 18, 2817–2854.

Şengör, A. M. C., & Natal'in, B. A. (1996). Turkic-type orogeny and its role in the making of the continental crust. *Annual Review of Earth and Planetary Sciences.*, 24, 263–337.

Shcheka, S. A. (1977). Meymechite–picritic complexes of the Sikhote-Alin. *Doklady Akademii Nauk SSSR*, 234(2), 444–447 (in Russian).

Shcheka, S. A. (1983). *Basite and hyperbasite intrusions and inclusions in effusives of Far East* (p. 165). Nauka (in Russian).

Shcheka, S. A., Volokhin, Y. G., & Karabtsov, A. A. (2009). The first finding of explosive alkaline picrites at Nadan'hada–Alin' (China). *Doklady Earth Sciences*, 429A(9), 1472–1477.

Shcheka, S. A., Vrzhosek, A. A., & Vysotskiy, S. V. (2003). Jurassic meymechite-picrite complexes of Primorye, Russia: Comparative study with komatiite and Japanese picrite suites. In N. V. Vladykin (Ed.), *Proceeding of International Workshop «Plumes and Problems of Deep Sources of Alkaline Magmatism»*, Khabarovsk (pp. 184–200). Publishing House of the Irkutsk State Technical University.

Simanenko, V. P., Khanchuk, A. I., & Golozoubov, V. V. (2002). First data on the geochemistry of Albian-Cenomanian volcanism in Southern Primorye, Russia's Far East. *Geochemistry International*, 40(1), 86–90.

Simonov, V. A., Prikhodko, V. S., Kovyazin, S. V., & Kotlyarov, A. V. (2014). Petrogenesis of meymechites of Sikhote Alin inferred from melt inclusions. *Russian Journal of Pacific Geology*, 8, 423–442.

Sun, S. -S., & McDonough, W. F. (1989). Chemical and isotopic systematics of oceanic basalts: Implications for mantle composition and processes. *Geological Society Special Publications*, 42, 313–345.

Tang, L. M., Chen, H. L., Dong, C. W., Yang, S. F., Shen, Z. Y., Cheng, X. G., & Fu, L. L. (2013). Middle Triassic post-orogenic extension on Hainan Island: Chronology and geochemistry constraints of bimodal intrusive rocks. *Science China Earth Sciences*, 56, 783–793.

Travin, A. V., Yudin, D. S., Vladimirov, A. G., Khromykh, S. V., Volkova, N. I., Mekhonoshin, A. S., & Kolotilina, T. B. (2009). Thermochronology of the Chernorudsky granulite zone, Ol'khon region, western Cisbaikalia. *Geochemistry International*, 47(11), 1107–1124.

Tsuchiya, N., Kimura, J. I., & Kagami, H. (2007). Petrogenesis of Early Cretaceous adakitic granites from the Kitakami Mountains, Japan. *Journal of Volcanology and Geothermal Research*, 167(1–4), 134–159.

Tsuchiya, N., Suzuki, S., Kimura, J. -I., & Kagami, H. (2005). Evidence for slab melt/mantle reaction: Petrogenesis of Early Cretaceous and Eocene high Mg andesites from the Kitakami Mountains, Japan. *Lithos*, 79, 179–206.

Tsutsumi, Y., Horie, K., Sano, T., Miyawaki, R., Momma, K., Matsubara, S., Shigeoka, M., & Yokoyama, K. (2012). LA-ICP-MS and SHRIMP ages of zircons in chevkinite and monazite tuffs from the Boso Peninsula, Central Japan. *Bulletin of the National Museum of Nature and Science, Series C*, 38, 15–32.

Tsutsumi, Y., Yokoyama, K., Kasatkin, S. A., & Golozoubov, V. V. (2016). Provenance study of accretionary complexes in Far East Russia using age and composition of detrital minerals. *Memoirs of the National Museum of Nature and Science*, 51, 79–87.

Wang, F., Xu, W. -L., Xu, Y. -G., Gao, F., & Ge, W. (2015). Late Triassic bimodal igneous rocks in eastern Heilongjiang Province, NE China: Implications for the initiation of subduction of the Paleo-Pacific Plate beneath Eurasia. *Journal of Asian Earth Sciences*, 97, 406–423.

Wang, K. X., Sun, T., Chen, P. R., Ling, H. F., & Xiang, T. F. (2013). The geochronological and geochemical constraints on the petrogenesis of the Early Mesozoic A-type granite and diabase in northwestern Fujian province. *Lithos*, 179, 364–381.

Wei, C., Wei, X., Zhu, W., & Xu, W. (2018). Petrogenesis of Early Cretaceous hornblende gabbro in Khanka Massif: Evidence from geochronology and geochemistry. *Global Geology*, 21(3), 166–176.

Wu, F. Y., Lin, J. Q., Wilde, S. A., Zhang, X. O., & Yang, J. H. (2005). Nature and significance of the Early Cretaceous giant igneous event in eastern China. *Earth and Planetary Science Letters*, 233(1–2), 103–119.

Wu, J. T. J., Jahn, B. M., Nechaev, V., Chashchin, A., Popov, V., Yokoyama, K., & Tsutsumi, Y. (2017). Geochemical characteristics and petrogenesis of adakites in Sikhote-Alin, Russian Far East. *Journal of Asian Earth Sciences*, 145, 512–529.

Xing, K. -C., Wang, F., Xu, W. -L., & Gao, F. -H. (2019). Tectonic affinity of the Khanka Massif in the easternmost Central Asian Orogenic Belt: Evidence from detrital zircon geochronology of Permian sedimentary rocks. *International Geology Review*, 62(4), 428–445.

Xu, W. -C., Luo, B. -J., Xu, Y. -J., Wang, L., & Chen, Q. (2018). Geochronology, geochemistry, and petrogenesis of late Permian to early Triassic mafic rocks from Darongshan, South China: Implications for ultrahigh-temperature metamorphism and S-type granite generation. *Lithos*, 308-309, 168–180.

Yamakita, S., & Otoh, S. (2000). Cretaceous rearrangement processes of pre-Cretaceous geologic units of the Japanese Islands by MTL-Kurosegawa left-lateral strike-slip fault system. *Memory of Geological Society of Japan*, 56(23–38), 2000.

Yang, J. H., & Wu, F. Y. (2009). Triassic magmatism and its relation to decratonization in the eastern North China Craton. *Science in China Series D Earth Sciences*, 52(9), 1319–1330.

Yi, S.-B., Oh, C. W., Lee, S.-Y., Choi, S.-G., Kim, T., & Yi, K. (2016). Triassic mafic and intermediate magmatism associated with continental

collision between the North and South China Cratons in the Korean Peninsula. *Lithos, 246-247*, 149–164.

Yokoyama, K., Tsutsumi, Y., & Das, K. (2010). Age distribution of monazites in sands collected from the most important rivers in Asia. *Memoirs of the National Museum of Nature and Science, 46*, 109–118.

Zakharov, V. A., Kurushin, N. I., & Pokhialainen, V. P. (1996). Paleo-biogeographic criteria of terrane geodynamics of Northeastern Asia in Mesozoic. *Russian Geology and Geophysics, 37*(11), 1–22.

Zheng, Y. -F. (2019). Subduction zone geochemistry. *Geoscience Frontiers, 10*, 1223–1254.

Zhou, J. -B., Wilde, S. A., Zhao, G. -C., Zhang, X. -Z., Zheng, C. -Q., Wang, H., & Zeng, W. -S. (2010). Pan-African metamorphic and magmatic rocks of the Khanka Massif, NE China: Further evidence regarding their affinity. *Geological Magazine, 147*(05), 737–749.

SUPPORTING INFORMATION

Additional supporting information may be found in the online version of the article at the publisher's website.